Properties of high-spin states in ^{91}Nb and ^{91}Zr via ^{6}Li-induced reactions*

B. A. Brown,† P. M. S. Lesser,‡ and D. B. Fossan
Department of Physics, State University of New York, Stony Brook, New York 11794
(Received 17 December 1975)

The properties of high-spin states in ^{91}Nb and ^{91}Zr have been studied with the ^{88}Sr(^{6}Li,$3n$)^{91}Nb and ^{88}Sr(^{6}Li,$p2n$)^{91}Zr reactions. In-beam measurements with Ge(Li) and Si(Li) detectors of γ-ray excitation functions, γ-γ coincidences, γ-ray angular distributions, and pulsed beam-γ timing spectra were made to establish decay schemes, level energies, spin-parity assignments, γ-ray multipolarities, and isomeric lifetimes. All of the high-spin states involving the $\pi 1g_{9/2}$, $\pi 2p_{1/2}$, and $\nu 2d_{5/2}$ orbitals as well as other more complicated states were identified. In particular, the theoretically predicted isomeric states in ^{91}Nb and ^{91}Zr were found: the $|(1g_{9/2})^2 2p_{1/2}, \frac{17}{2}^-\rangle$ state in ^{91}Nb is at 2035 keV with a $\tau = 5.42 \pm 0.18$ μsec, and the $|(1g_{9/2})^2 2d_{5/2}, \frac{21}{2}^+\rangle$ state in ^{91}Zr is at 3167 keV with a $\tau = 6.28 \pm 0.20$ μsec. The experimental energy levels and $B(E2)$ values obtained for these nuclei as well as those of other $N = 50$ and 51 nuclei are compared with recent theoretical work of Gloeckner *et al.* The $E2$ effective charges for the mass-90 region are discussed.

[NUCLEAR REACTIONS ^{88}Sr(^{6}Li, $3n$), ^{88}Sr(^{6}Li, $p2n$), $E = 34$ MeV, pulsed beam; measured γ-γ coincidence; deduced levels in ^{91}Nb and ^{91}Zr; measured $\gamma(E, \theta, t)$; deduced J^π, $T_{1/2}$, branching ratio, $\delta(E2/M1)$, $B(E2)$, effective charges. Natural target, Ge(Li) and Si(Li) detectors.]

I. INTRODUCTION

The nuclei surrounding ^{90}Zr have simple shell-model descriptions because of the good $N = 50$ neutron shell closure and the partial proton shell closure at $Z = 38$. Many levels in the $N = 50$ nuclei beyond $Z = 38$ can be described in first order by proton configurations in the $1g_{9/2}$ and $2p_{1/2}$ orbitals. The $N = 49$ and $N = 51$ nuclei are described similarly by the coupling of a $1g_{9/2}$ neutron-hole orbital and a $2d_{5/2}$ neutron-particle orbital, respectively, to the $N = 50$ configurations. The mass-90 region is one of several spherical nuclear regions such as the regions near ^{16}O, ^{40}Ca, and ^{208}Pb which provide a variety of tests for the many-body theories. In particular, they give a relatively direct test of the microscopic nuclear models which constitute one of the most fundamental approaches to the many-body problem.

High-spin states in the spherical nuclei are particularly simple to describe because of the limited number of possible shell-model configurations. Even before 1960 many high-spin states in ^{90}Zr were known[1] and interpreted with an effective two-body operator in terms of $(2p_{1/2}, 1g_{9/2})^2$ configurations.[2] The theoretical studies up to 1966 were culminated in two shell-model calculations by Vervier[3] and Auerbach and Talmi[4] in which a large body of data for the Y, Zr, Nb, Mo, and Tc isotopes was interpreted in terms of effective two-body matrix elements as opposed to effective two-body operators. Among other things, the known isomeric level in ^{93}Mo[5] was explained by these calculations. Because of this success, other isomeric levels in ^{91}Nb and ^{91}Zr that resulted from these calculations were predicted with some confidence.

More recently experimental information on mass-90 high-spin states has been obtained with α- and light-particle-induced reactions. The most extensive of these investigations was by Lederer and co-workers[6] for the Mo and Ru isotopes and by the Stockholm group for several $N = 49$, 50, and 51 nuclei.[7,8] These in turn led recently to more complete shell-model calculations for the mass-90 region.[9-12] One of the main aims of the recent theoretical calculations was to explain the properties of a large region of nuclei with one consistent set of two-body interaction matrix elements and one-body electromagnetic operators assuming only a few active orbitals in the model space. A small model space has the advantage of restricted degrees of freedom which result in calculations that are not limited by the number of particles within the model space.

Considerable experimental information regarding the high-spin states in the mass-90 region, however, remained unknown even for some of the simplest nuclei such as ^{91}Nb, ^{91}Zr, ^{92}Nb, and ^{92}Zr. For example, the predicted ^{91}Nb and ^{91}Zr isomeric states had not been seen. These nuclei with only a few active nucleons are important not only to serve as a further test of the existing shell-model calculations, but also because if the discrepancies between experiment and theory are to be explained by a more extensive calculation in

which more active orbitals are included, only these simpler nuclei can reasonably be considered. Shell-model calculations within a large model space are severely limited by the number of active nucleons.

In order to obtain the more complete experimental information on high-spin states in the mass-90 region, a series of experiments was undertaken using previously unexploited ^{6}Li- and ^{7}Li-induced fusion-evaporation reactions. These reactions gave the proper high-spin selectivity for γ-ray spectroscopy in nuclei of $\Delta Z \leq 3$ relative to available stable targets. Lighter-particle-induced reactions in most cases do not populate the high-spin states with sufficient strength for experimental measurements and some residual nuclei of interest cannot be reached in this way from stable targets. In the present fusion-evaporation reactions,[13] the Li ions bring a large orbital angular momentum into the fused compound system and the subsequent evaporation of low-energy nucleons, which carry away only a small angular momentum, results in the population with large cross sections of high-spin states in the residual nuclei. The dominant decay mode of these states is via stretched γ-ray cascades $J \rightarrow J - L$ down through the yrast levels, which are the lowest energy states for the various existing values of J^{π}. Because the orbital angular momentum brought into the compound system by the Li ions is perpendicular to the beam direction, the populated high-spin states are strongly aligned in low-m substates relative to the beam axis. This alignment results in strongly anisotropic γ-ray angular distributions which are characteristic of the multipolarity L of the γ-ray transitions. The γ-ray transitions following these Li-induced fusion-evaporation reactions thus contain the information needed to establish the level schemes in the residual nuclei including J^{π} values and the decay properties of the high-spin states. To extract this information, several different in-beam γ-ray experiments were performed: (1) γ-ray excitation measurements, (2) γ-γ coincidence measurements, (3) γ-ray angular distribution measurements, and (4) pulsed beam-γ timing measurements.

In the present paper, the experimental results for ^{91}Nb and ^{91}Zr obtained from the ^{88}Sr(^{6}Li, $3n$)^{91}Nb and ^{88}Sr(^{6}Li, $p2n$)^{91}Zr reactions are presented. The level scheme and decay properties of all of the high-spin states in these nuclei involving the $\pi 1g_{9/2}$, $\pi 2p_{1/2}$, and $\nu 2d_{5/2}$ orbitals as well as more complicated high-spin states were obtained. In particular, the theoretically predicted isomeric levels in both ^{91}Nb and ^{91}Zr were found: the $|(1g_{9/2})^2 2p_{1/2}, \frac{17}{2}^-\rangle$ state in ^{91}Nb was located at 2035 keV and its mean lifetime was measured to be $\tau = 5.42 \pm 0.18$ μsec, and the $|(1g_{9/2})^2 2d_{5/2}, \frac{21}{2}^+\rangle$ state in ^{91}Zr was located at 3167 keV and its mean lifetime was measured to be $\tau = 6.28 \pm 0.20$ μsec. Preliminary results of some of the present work have been reported previously.[14,15] Experimental results for other mass-90 nuclei are to be published separately.[16] ^{92}Nb has been studied with the ^{88}Sr(^{7}Li, $3n$)^{92}Nb reaction, ^{92}Zr with ^{88}Sr-(^{7}Li, $p2n$)^{92}Zr, ^{93}Tc with ^{90}Zr(^{6}Li, $3n$)^{93}Tc, ^{93}Mo with ^{90}Zr(^{6}Li, $p2n$)^{93}Mo, and ^{95}Ru with ^{92}Mo-(^{6}Li, $p2n$)^{95}Ru.

Previously available information concerning ^{91}Nb and ^{91}Zr, which was obtained mostly by light ion reactions and β decay studies is summarized in Nuclear Data Sheets.[17] Spin assignments from these investigations were limited to $J \leq \frac{11}{2}$. Recent studies of ^{91}Nb which are relevant to the yrast levels discussed in the present paper utilized the reactions ^{91}Zr($p, n\gamma$),[18] ^{90}Zr(p, γ),[19] ^{89}Y($\alpha, 2n\gamma$),[20] and ^{90}Zr($\alpha, p2n\gamma$).[7] Results for the ^{91}Nb isomeric state consistent with the present experiment have also recently been reported.[21] Studies of ^{91}Zr pertaining to the yrast levels have utilized the reactions ^{91}Zr(p, p'),[22] ^{90}Zr(d, p),[22-24] ^{90}Zr($d, p\gamma$),[24] and ^{88}Sr($\alpha, n\gamma$).[20,25]

The details of the present experimental measurement are described in Sec. II and the experimental results for ^{91}Nb and ^{91}Zr are presented in Sec. III. In Sec. IV the deduced energy levels and electromagnetic matrix elements are compared with the recent theoretical calculation of Gloeckner *et al.*[10-12]

II. EXPERIMENTAL TECHNIQUE

Levels in ^{91}Nb and ^{91}Zr were populated by means of the fusion-evaporation reactions ^{88}Sr(^{6}Li, $3n$)^{91}Nb and ^{88}Sr(^{6}Li, $p2n$)^{91}Zr. For most of the measurements, a 34-MeV ^{6}Li (3^+) beam, obtained from the Stony Brook FN tandem Van de Graaff accelerator, was incident on a thick natural Sr metal target (82.6% ^{88}Sr) which stopped the beam. Deexcitation γ rays were detected in these studies with Ge(Li) and Si(Li) detectors having energy resolutions of 2.5–3 keV and 180 eV FWHM (full width at half maximum), respectively.

In fusion-evaporation reactions[13] such as (^{6}Li, $3n$), the incident heavy ion carries a large amount of angular momentum into the compound system ($l \cong 17\hbar$ for a classical grazing collision of 34-MeV ^{6}Li on ^{88}Sr); the evaporation nucleons, on the other hand, carry away relatively little angular momentum, amounting to, at most, a few $\hbar$ per nucleon. This has two important consequences: (1) the reaction mechanism favors the population of high-spin states in the residual nucleus, and (2) these states are formed with a

high degree of alignment (low-m substate population), since the incoming orbital angular momentum is oriented perpendicular to the incident beam direction ($m_i = 0$). The dominant decay mode of these states is via stretched γ-ray cascades, $J \rightarrow J - L$ where J and $J - L$ are the initial and final level spins and L is the multipolarity of the γ-ray transitions. Thus both the excitation and deexcitation mechanisms tend selectively to involve only the yrast levels,[13] which are the lowest-lying levels for a given spin.

The experimental techniques utilized for these γ-ray measurements in the determination of level schemes and electromagnetic decay properties of ^{91}Nb and ^{91}Zr are discussed below.

A. γ-ray excitation measurements

Measurements of the characteristic γ-ray yields as a function of excitation energy for the fusion-evaporation reactions can provide an aid in the identification of the γ rays originating in the various residual nuclei. In addition, the γ-ray excitation function allows the determination of the optimum bombarding energy for the γ-ray measurements relating to the specific residual nucleus.

The (HI, xn) cross sections for the population of high-spin states have a characteristic peak for each x, the number of evaporated neutrons, as a function of bombarding energy. These features are understood on the basis of theoretical calculations and observed systematics for a large amount of reaction data.[13] An empirical estimate of the bombarding energy for the peak cross section[13] is $E_{pk}(x) = (1 + A_1/A_2)(-Q_x + 6x)$ MeV where A_1 and A_2 refer to the masses of the bombarding heavy ion and the target nucleus, respectively, and Q_x is the Q value for the (HI, xn) reaction. An energy of $6x$ MeV is allowed for the evaporation of the x neutrons. The widths for these cross sections peaks are typically 10–15 MeV FWHM; thus, the γ-ray yields from the various residual nuclei specified by x can, to a large extent, be separated by the choice of bombarding energy. The fusion-evaporation reactions, for which one of the evaporated nucleons is a proton, show a less distinctive cross section dependence because of penetration effects of the Coulomb barrier for the proton. The cross section peak, however, is displaced upward by roughly the Coulomb-barrier energy.

Measurements of γ-ray excitation functions for several mass-90 targets (^{88}Sr, ^{89}Y, ^{90}Zr, ^{92}Mo) have been made with ^{6}Li and ^{7}Li beams. The γ-ray spectra were measured in a Ge(Li) detector positioned at 90° in an energy range of interest above the Coulomb barrier up to 35 MeV. The yields for γ rays associated with specific residual nuclei were observed to follow the above discussed cross section features. For the present study, the estimated peak energy for the ^{88}Sr(^{6}Li, $3n$)^{91}Nb reaction is $E_{pk}(x = 3) = 31$ MeV while for the ^{88}Sr(^{6}Li,$2n$)-^{92}Nb reaction, $E_{pk}(x = 2) = 17$ MeV. Because of the difficulty of maintaining thin self-supporting Sr targets, most of the γ-ray measurements were made with thick natural Sr metal targets at a ^{6}Li energy of 34 MeV. At this energy, the ^{88}Sr(^{6}Li,$3n$)-^{91}Nb yield was maximized and an adequate yield for the study of ^{91}Zr was also achieved from the ^{88}Sr(^{6}Li, $p2n$)^{91}Zr reaction, which has an estimated peak energy of 37 MeV. The thick-target yields at 34 MeV for these reactions and other reaction channels are given in Sec. III.

B. γ-γ coincidence measurements

The thick-target yields from the (^{6}Li, $3n$) and (^{6}Li, $p2n$) reactions were relatively large at the incident beam energy of 34 MeV; however, yields from other reactions, especially ^{88}Sr(^{6}Li, αn)^{89}Y and ^{88}Sr(^{6}Li, $\alpha 2n$)^{88}Y, were appreciable. This fact, plus the fact that the target was not isotopically pure, resulted in complex singles γ-ray spectra. Thus, the identification of γ-ray transitions from a particular nucleus required the use of γ-γ coincidence measurements.

The detector systems employed for these measurements consisted of two large volume Ge(Li) detectors for γ rays in the range ~100 keV to several MeV and a Ge(Li)-Si(Li) detector system for coincidence events involving very low energy γ rays. The detectors were placed at 90° and −120° with respect to the beam direction in order to reduce coincidences from annihilation radiation. Standard fast-slow electronics were employed and the data were recorded on magnetic tape in a three-parameter [energy No. 1, energy No. 2, and time-to-amplitude (TAC) signal] event-by-event mode. Subsequent scanning of the data tapes for prompt events (±100 nsec) and with digital windows set on specific full energy peaks generated the coincidence spectra. Scans could be generated for both true and random coincidences, based on the TAC window, although random coincidences were found to be negligible in all cases. Compton background was subtracted by setting windows on appropriate regions above or below the full energy peaks. A total of $\sim 5 \times 10^6$ events were recorded on magnetic tape and analyzed.

C. γ-ray angular distributions

Information regarding transition multipolarities and relative γ-ray intensities was obtained from

measurements of the γ-ray angular distributions. This information was valuable in making spin assignments and in determining the sequence of γ-ray transitions in ^{91}Nb and ^{91}Zr. Branching ratios were extracted as well as some mixing ratios for several transitions.

The angular distribution data were taken with a Ge(Li) detector at seven equally spaced angles between 0° and 90° with respect to the beam. A monitor detector was placed at −90° for the purpose of normalization; dead-time corrections were made by running a beam current dependent pulser into both detectors. Beam-off measurements of long-lived activity lines were used to correct for anisotropies in the experimental geometry. The Ge(Li) relative detection efficiency vs energy was measured with several radioactive sources. This information was needed to extract relative γ-ray intensities I_γ from the integrated angular distributions.

The angular distributions, based on extracted photopeak areas, were fitted with the function

$$W(\theta_\gamma) = I_\gamma [1 + A_2 P_2(\cos\theta_\gamma) + A_4 P_4(\cos\theta_\gamma)] ,$$

where P_2 and P_4 are the usual Legendre polynomials and the coefficients A_2 and A_4 are dependent upon the multipolarity of the transition as well as the degree of alignment of the decaying state. These coefficients have been calculated[26] assuming complete alignment, i.e., population of $m=0$ or $m=\pm\frac{1}{2}$ substates only, for integer or half-integer spins, respectively. Since the fusion-evaporation reaction mechanism allows a finite spread in m-substate population, as does cascade γ-ray feeding, the experimentally determined coefficients A_k are attenuated by a factor, which will be denoted by α_k in the tables, from those calculated assuming complete alignment.

The most unambiguous spin and parity assignment that can be made for prompt transitions ($\tau \lesssim 10$ nsec) on the basis of angular distribution information alone occurs for the case of a stretched-quadrupole $J \to J-2(E2)$ cascade. These are characterized by a coincident set of γ rays which have about the same positive A_2 and negative A_4 coefficients and whose intensities show a regular decrease as their position increases in the cascade. Typically, $A_2 \approx 0.3$ and $A_4 \approx -0.1$. Strong spin assignments that are unbracketed in the figures will be made for these cases. In addition, strong spin and parity assignments will be made in cases, which will be individually explained, where the angular distribution information can be supplemented by lifetime and branching information.

A stretched-dipole $J \to J-1$ transition would be characterized in a similar way by a coincident set of γ rays, which have about the same negative A_2 coefficients and zero A_4 coefficients, and whose intensities show a regular decrease. Typically, $A_2 \approx -0.2$. However, for $M1$ transitions these angular distributions are not always realized in their pure form since the A_2 coefficient is very sensitive to $E2$ admixtures which often compete. Spin assignments based on this type of transition will be considered tentative and bracketed in the figures. The situation is especially tentative for the weak transitions which may originate from nonyrast levels and which often have large errors in the angular distribution coefficients.

In a few cases, the measured angular distributions have been fitted assuming a mixed transition to determine the mixing ratio. The phase convention used for the mixing ratio is the same as that used by Yamazaki.[26] These determinations depend rather sensitively on the assumed m-substate population for the decaying state. It has been found[27] that for fusion-evaporation reactions the actual m-substate population can be adequately described by a Gaussian distribution of the form:

$$P_J(m) = \frac{\exp(-m^2/2\sigma^2)}{\sum_{m'=-J}^{J} \exp(-m'^2/2\sigma^2)} .$$

This form was used in fitting the present data, by using a width parameter σ that was extracted from fits to transitions for which J_i, J_f, and the mixing ratio were known. To the extent that consistent values for σ were obtained (see Table II) at least for levels of about the same excitation energy and spin, reliable mixing ratios were determined. The mixing ratios are subject to the qualification that the γ ray observed in singles can be isolated at each angle from all background γ rays. This assumption is difficult to check due to the complex γ spectra which may contain doublets that are not resolved.

D. Pulsed beam-γ measurements

The search for isomeric γ-ray transitions was conducted with the Stony Brook beam pulsing system, which supplied 34-MeV ^{6}Li beam pulses having a width of $\lesssim 2$ nsec and repetition periods ranging from 250 nsec to 32 μsec. A reference signal derived from the beam deflector was used as the "stop" signal for a time-to-amplitude converter (TAC); the "start" signal was obtained from the γ-ray detector. Using standard fast electronics, an over-all system time resolution of ~8 nsec FWHM was obtained for a dynamic range in γ-ray energy of about 10:1. Lifetime measurements were carried out over a time range of about 20 nsec to 500 μsec. The advantage of

the pulsed beam technique, compared with delayed coincidence measurements, is that data are taken at essentially singles counting rates rather than the much slower two-detector coincidence rates.

In the present experiments, delayed γ-ray spectra were obtained by setting windows on portions of the TAC spectrum and recording the corresponding energy spectra. Lifetimes were obtained from the relative intensities of γ-ray lines (full energy peaks) in two or more known time regions. This method of measuring lifetimes was found to be preferable to direct measurement of the expo-

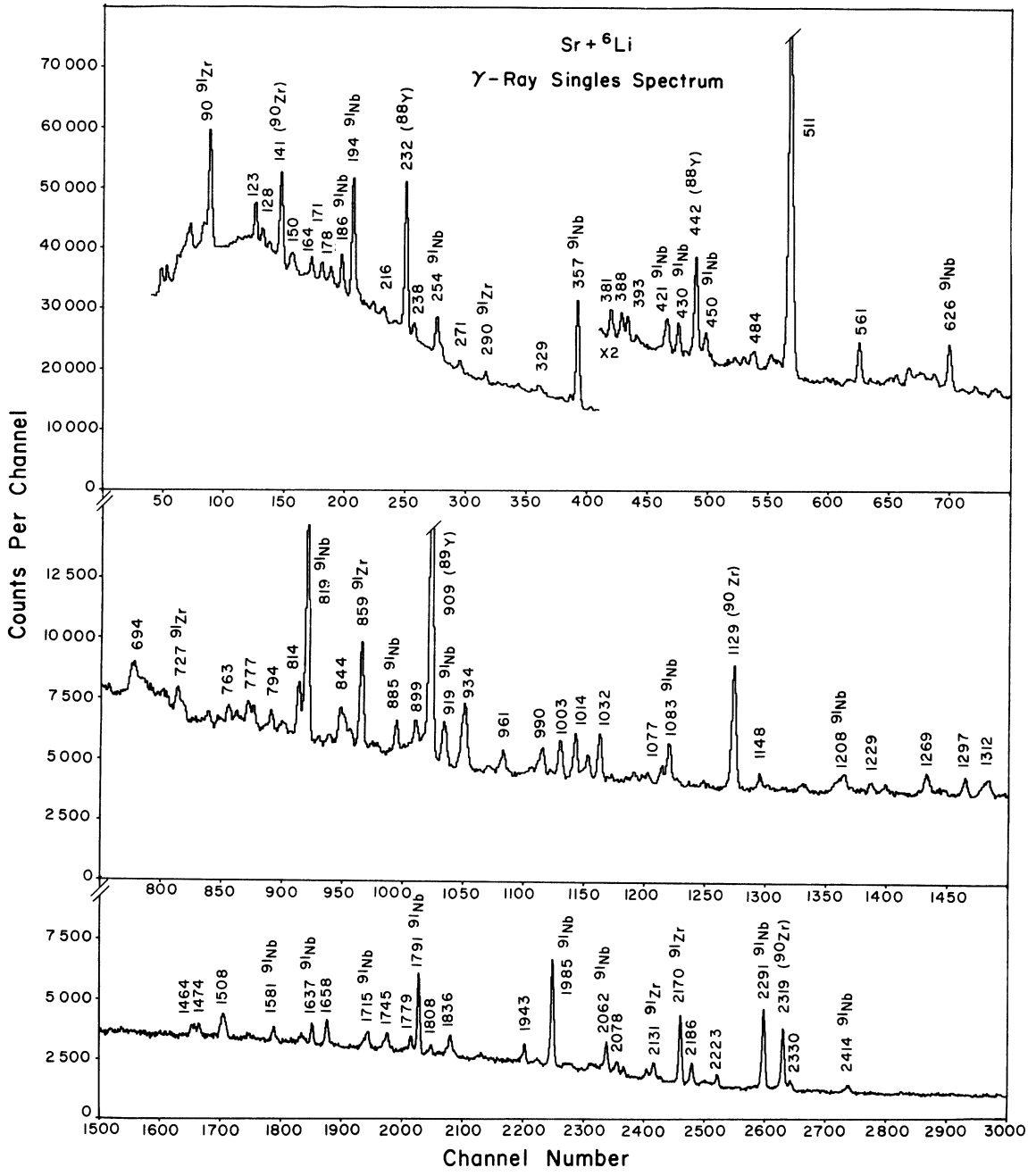

FIG. 1. The Ge(Li) γ-ray singles spectrum from natural Sr(82.6% ^{88}Sr) + ^{6}Li at 34 MeV. A thick metallic target was used. All strong γ rays which have been associated with ^{91}Nb or ^{91}Zr are labeled with the corresponding nucleus. A few of the strongest γ rays from other nuclei are indicated although the origin of most others not specifically labeled by a nucleus are known. At channel number 1500, the channel scale has been changed by a factor of 2.

nential decay curve for lifetimes in the μsec range, because of the greater ease with which background could be subtracted. In addition, this technique permitted immediate identification of all lines having delayed components, i.e., all those associated with the decay of isomeric states.

III. EXPERIMENTAL RESULTS

The singles γ-ray spectrum from the reactions induced by a 34-MeV ^{6}Li beam on a thick natural Sr metal target is shown in Fig. 1. This choice of energy, which gave the maximum relative yield for ^{91}Nb with the thick target, is consistent with the observed thin-target excitation functions mentioned earlier. γ rays from the following nuclei were observed with the relative yields estimated from all previously known transitions to the respective ground states: ^{91}Nb (17), ^{89}Y (7), ^{91}Zr (5), ^{90}Zr (5), ^{88}Y (3), ^{88}Sr (1), and ^{92}Zr (1). In addition γ transitions from the nuclei ^{92}Nb, ^{91}Y, ^{90}Nb, ^{90}Y, ^{88}Z, ^{87}Sr, ^{87}Y, ^{86}Sr, and ^{84}Sr were weakly observed. The strongest reactions are for the isotope ^{88}Sr (82.6%): ^{88}Sr(^{6}Li, $3n$)^{91}Nb, ^{88}Sr-

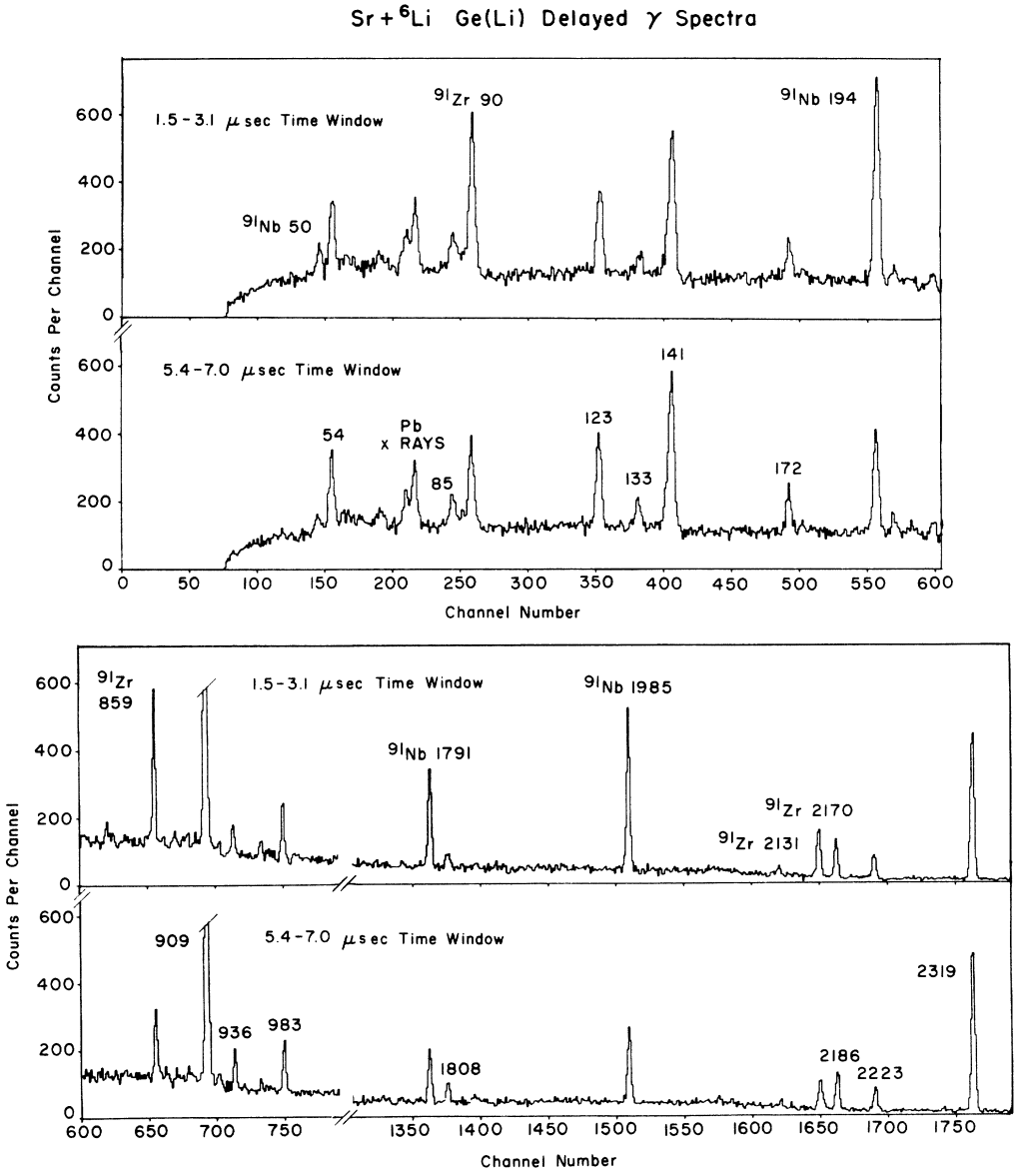

FIG. 2. Delayed Ge(Li) γ spectra from the Sr + ^{6}Li reactions integrated over two equal time regions, 1.5–3.1 μsec and 5.4–7.0 μsec. γ rays from ^{91}Nb and ^{91}Zr are labeled in the first time window. There is a gain change between the top and bottom halves of the figure.

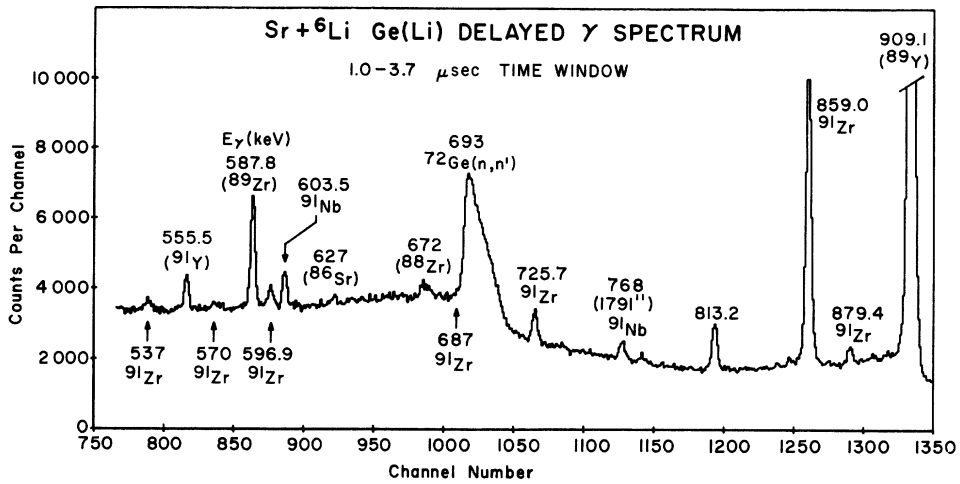

FIG. 3. A portion of the delayed Ge(Li) γ spectrum from the Sr + ^{6}Li reactions taken with better statistics than the spectra shown in Fig. 2 to show the weak delayed γ rays in ^{91}Nb and ^{91}Zr. The origins of the other delayed γ rays are also indicated.

(^{6}Li, $p2n$)^{91}Zr, ^{88}Sr(^{6}Li, $p3n$)^{90}Zr, ^{88}Sr(^{6}Li, αn)^{89}Y, and ^{88}Sr(^{6}Li, $\alpha 2n$)^{88}Y. Part of the yield for the other nuclei comes from ^{6}Li reactions with the other naturally occurring Sr isotopes: ^{87}Sr (7.0%), ^{86}Sr (9.9%), and ^{84}Sr (0.6%).

Other than the results for ^{91}Nb and ^{91}Zr, which are presented in detail in this section, no new results were obtained for other nuclei. The present results for ^{88}Y and ^{89}Zr are consistent with and confirm previous data for the high-spin states in these nuclei.[8,28] A pulsed beam-delayed γ measurement for the 122-keV γ ray yielded a mean lifetime of $\tau = 87 \pm 4$ μsec for the 122-keV 6^{+} level in ^{90}Nb which is in good agreement with a previous measurement of $\tau = 88 \pm 6$ μsec.[29]

New isomeric levels were found in both ^{91}Nb and ^{91}Zr with mean lifetimes of $\tau = 5.42 \pm 0.18$ μsec and $\tau = 6.28 \pm 0.20$ μsec, respectively. Delayed γ spectra, which are integrated over time regions sensitive to these lifetimes, are shown for the Ge(Li) detector in Figs. 2 and 3 for the Si(Li) detector in Fig. 4. The energies and intensities

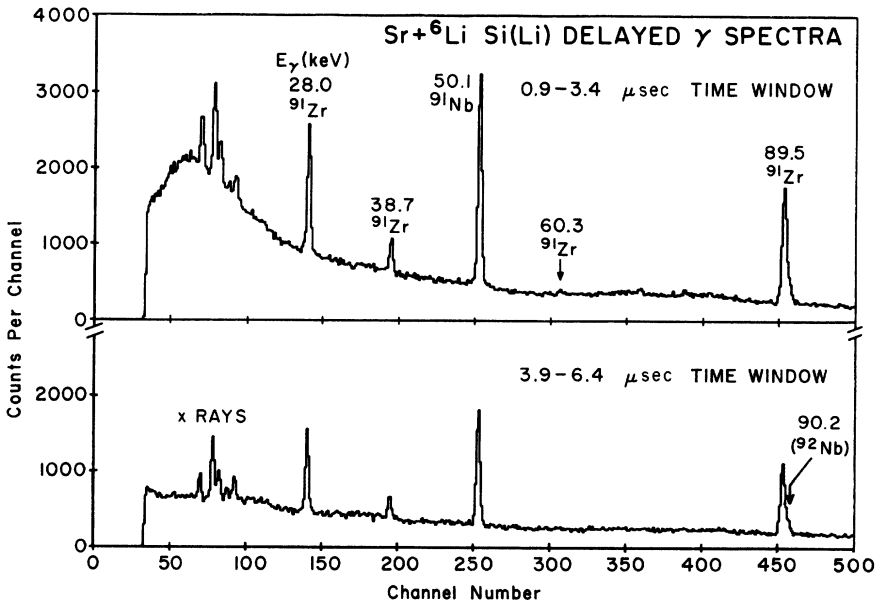

FIG. 4. Delayed Si(Li) γ spectra from the Sr + ^{6}Li reactions integrated over two equal time regions, 0.9–3.4 μsec and 3.9–6.4 μsec. A thin Al absorber was placed in front of the detector to reduce the intense prompt x rays.

of the γ rays in these delayed spectra were most valuable in determining the position and decay modes of the isomers in ^{91}Nb and ^{91}Zr. The intensities of the predominant delayed γ rays were obtained from angular distribution measurements at 0°, 45°, and 90°. The angular distribution coefficients were found to be attenuated in the delayed region due to hyperfine interactions in the Sr metal; the observed A_2 coefficients were attenuated by about 75% in the 5–7-μsec delayed region.

The γ-γ coincidence results for transitions in ^{91}Nb and ^{91}Zr are listed in Table I for the combinations of Ge(Li)-Ge(Li) and Ge(Li)-Si(Li) detectors. The γ-γ coincidence data were especially important in constructing the decay scheme for prompt ($\tau \lesssim 5$ nsec) transitions in ^{91}Nb. Some of the typical γ-γ coincidence spectra for ^{91}Nb γ rays are shown in Fig. 5.

The angular distribution coefficients A_2 and A_4 extracted from the angular γ-ray singles measurements, which include both delayed and prompt components, are given in Tables II and III for ^{91}Nb and ^{91}Zr, respectively. These results were used to determine γ-ray multipolarities and spin information. For the prompt transitions in ^{91}Nb, quantitative information concerning the m-substate population parameters was obtained leading to some mixing ratios. The prompt and the delayed γ-ray intensities obtained from the angular distribution measurements are also given in Tables II and III.

In the following subsections the present results for ^{91}Nb and ^{91}Zr are discussed. The level scheme obtained for ^{91}Nb is shown in Fig. 6 and the γ-ray decay properties are summarized in Table II. The level scheme and γ-ray decay properties for ^{91}Zr are given in Fig. 7 and Table III, respectively.

A. ^{91}Nb isomeric decay

Three γ rays with energies 194, 1791, and 1985 keV, that were known to be from ^{91}Nb, appeared with large intensities in the μsec-delayed γ-ray spectra all displaying a similar time dependence (see Fig. 2) which yielded a mean lifetime of τ

TABLE I. Results of γ-γ coincidence measurements for ^{91}Nb and ^{91}Zr.

γ ray in gate (keV)	Coincident γ rays[a] (keV)
^{91}Nb Ge(Li)-Ge(Li)	
186	254, 357, 421, (497), 819, (885), 2062, 2291
194	50, 430, (624), 1791
254	186, 421, 919, 2062
357	186, (421), 450, (626), 819, 885, 2291
421	184, (186), 254, (258), 357, 497, 822, (1060), 2062
430	194, 1791, (1985)
450	357, 626
626	305, 357, 450
819	186, 357, (817), 885, 919, 2291
885	(166), 184, (186), 357, 421, 819, 919, 2291
919	140, 186, 254, 817
1715	357
1791	(50), 194, 651
1985	50
2062	186, 254, 421
2291	(186), 357, 819, 885, 1014
^{91}Nb Si(Li)-Ge(Li)	
50	1791, 1985
^{91}Zr Ge(Li)-Ge(Li)	
90	477, (597), 859, 2131, 2170, (2350)
290	726
726	290, 2131
859	90, 2170
2131	39, (90), 230, (290), 726
2170	60, 90, 859
^{91}Zr Si(Li)-Ge(Li)	
28	859, 2170
90	859, 2170

[a] Relatively strong coincidences are underlined and coincidences which are uncertain are bracketed.

$= 5.42 \pm 0.18$ μsec. These γ rays are associated with the $\frac{13}{2}^- \rightarrow \frac{9}{2}^-$, $\frac{9}{2}^- \rightarrow \frac{9}{2}^+$, and $\frac{13}{2}^- \rightarrow \frac{9}{2}^+$ transitions (see Fig. 6), respectively, on the basis of the present as well as previous measurements.[17-20] These γ rays all exhibited a prompt component; however, a 50.1-keV delayed γ ray with the same lifetime which had no prompt component was observed with a Si(Li) detector (see Fig. 4). In the γ-γ data, the 50-keV γ ray was in coincidence with the 194-, 1791-, and 1985-keV γ rays. Thus the isomeric decay is due to a level at 2035 keV. The transition strength for the 50-keV transition to the $\frac{13}{2}^-$ level is consistent with a normally enhanced single-particle $E2$ decay [taking into account the theoretical internal conversion coefficient[30] (ICC) of 13.9] which implies a spin assignment of $\frac{17}{2}^-$ for the 2035-keV level. A recent measurement of the delayed Nb K-shell ICC with the ^{89}Y$(\alpha, 2n)^{91}$Nb reaction[21] gave a value consistent with that expected for a 50.1-keV $E2$ transition.

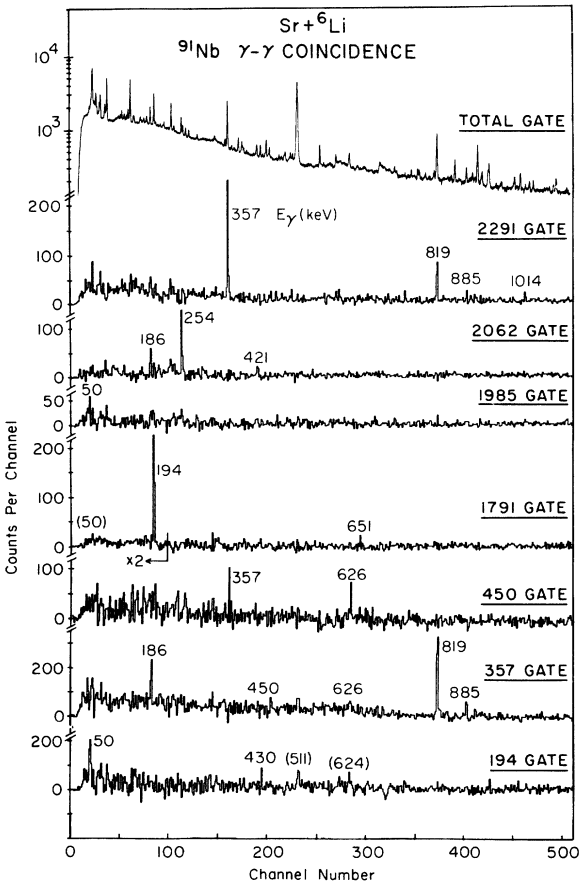

FIG. 5. γ-γ coincidence spectra from the Sr + ^{6}Li reactions using a Ge(Li)-Ge(Li) detector combination. Selected spectra for ^{91}Nb γ rays are shown. See Table I for a complete listing of the coincidence results for the ^{91}Nb and ^{91}Zr γ rays.

In addition to the above isomeric information, the decay γ rays from the 1985-keV $\frac{13}{2}^-$ state exhibited a shorter component of $\tau \approx 15$ nsec. In a previous ^{89}Y$(\alpha, 2n)^{91}$Nb experiment, a mean lifetime of $\tau = 14.4 \pm 0.5$ nsec was observed for the 1985-keV γ ray and attributed to another cascade γ ray which had a similar delay.[20] However, this cascade γ ray was not observed in the present experiment and was subsequently found to originate from a target contaminant in the ^{89}Y-$(\alpha, 2n)^{91}$Nb experiment.[20] Thus the $\tau = 14.4$-nsec mean lifetime must be attributed to the 1985-keV $\frac{13}{2}^-$ level.

The isomeric decay for the 2035-keV $\frac{17}{2}^-$ level in ^{91}Nb is shown on the left side of Fig. 6. A branching ratio of $(62 \pm 1)\%$ was obtained for the $\frac{13}{2}^- \rightarrow \frac{9}{2}^+$ transition. In addition to the strong γ rays discussed above, 603- and 1083-keV γ rays appeared weakly in the delayed spectra giving a branching ratio of $(3.5 \pm 0.5)\%$ for the 1791-keV $\frac{9}{2}^- \rightarrow$ 1187-keV $\frac{5}{2}^-$ transition.

B. ^{91}Nb prompt decay

The prompt decay mode and spin assignments for levels up to 5182 keV (see Fig. 6) have been determined from the γ-γ coincidence and angular distribution measurements. The three strongest coincident γ rays, 357, 819, and 2291 keV, were assigned to the stretched $E2$ cascade 3467-keV $\frac{21}{2}^+ \rightarrow$ 3110-keV $\frac{17}{2}^+ \rightarrow$ 2291-keV $\frac{13}{2}^+ \rightarrow$ g.s. $\frac{9}{2}^+$ on the basis of their relative intensities and angular distributions (Table II). These assignments are in agreement with previous experiments.[7,21]

The sum of the energies of the 450- and 626-keV γ rays which make up a coincident triplet with the 357-keV transition suggests a cascade from the $\frac{17}{2}^+$ to the $\frac{17}{2}^-$ state. The singles intensities give the intermediate state at 2661 keV and a spin of $\frac{15}{2}$ or $\frac{19}{2}$ is suggested by the fact that the 450- and 626-keV γ rays have angular distributions characteristic of $\Delta J = \pm 1$ dipole transitions. The thick-target Doppler shift observed at 0° for the 626-keV γ ray as opposed to a lack of Doppler shifts observed for the 357-, 450-, 819-, and 885-keV $E1$ and $E2$ transitions, indicate a fast $M1$ transition ($\tau \lesssim 20$ psec) for this γ ray which implies a negative parity for the 2661-keV level.

A previous assignment of a 626-keV γ ray to the 2414-keV $\frac{11}{2}^- \rightarrow$ 1791-keV $\frac{9}{2}^-$ transition[21] is not supported by the present experiment. The 430- keV and 2414-keV branches from the 2414-keV level[18,21] were observed in the present experiment, the 430-keV γ ray being in coincidence with the 194-keV γ ray. However, the 626-keV γ ray (or one with a slightly lower energy of 624

TABLE II. Properties of γ rays assigned to transitions in ^{91}Nb from the ^{88}Sr(^{6}Li, $3n$)^{91}Nb reaction.

E_γ (keV)	Total intensity [a] (Relative units)	Isomeric intensity [a] (Relative units)	A_2	A_4	Transition assignment $E_i \rightarrow E_f$ (keV) (keV)	$J_i^\pi \rightarrow J_f^\pi$	Other properties [b]
50.1 ± 0.2	~6	~6			2035 → 1985	$\frac{17}{2}^- \rightarrow \frac{13}{2}^-$	
194.1 ± 0.3	48	31 [c]	0.22 ± 0.02	−0.06 ± 0.03	1985 → 1791	$\frac{13}{2}^- \rightarrow \frac{9}{2}^-$	$\alpha_2(\frac{13}{2}^-) = 0.50 \pm 0.05$; $\alpha_4(\frac{13}{2}^-) = 0.27 \pm 0.14$
254.5 ± 0.5	13		−0.29 ± 0.03	0.01 ± 0.03	4352 → 4097	$(\frac{21}{2}^-) \rightarrow (\frac{19}{2}^-)$	
356.7 ± 0.3	56		0.35 ± 0.02	−0.09 ± 0.02	3467 → 3110	$\frac{21}{2}^+ \rightarrow \frac{17}{2}^+$	$\sigma(\frac{21}{2}^+) = 2.45 \pm 0.35$
429.6 ± 0.5	9		0.27 ± 0.04	0.04 ± 0.05	2414 → 1985	$\frac{11}{2}^- \rightarrow \frac{13}{2}^-$	$\delta(E2/M1) = -0.42 \pm 0.05$ with $\sigma(J_i) = 2.0 \pm 0.3$
449.6 ± 0.5	7		−0.22 ± 0.10	−0.06 ± 0.11	3110 → 2661	$\frac{17}{2}^+ \rightarrow (\frac{15}{2}^-, \frac{19}{2}^-)$	
603.5 ± 0.3	Weak	1.2 [d]			1791 → 1187	$\frac{9}{2}^- \rightarrow \frac{5}{2}^-$	
626.3 ± 0.5	15		−0.16 ± 0.05	0.03 ± 0.06	2661 → 2035	$(\frac{15}{2}^-, \frac{19}{2}^-) \rightarrow \frac{17}{2}^-$	$\delta(E2/M1) = -0.02 \pm 0.05$ for $J_i = \frac{15}{2}$ with $\sigma(J_i) = 2.0 \pm 0.3$; $\delta(E2/M1) = 0.06 \pm 0.05$ for $J_i = \frac{19}{2}$ with $\sigma(J_i) = 2.0 \pm 0.3$
819.4 ± 0.3	69		0.39 ± 0.02	−0.12 ± 0.03	3110 → 2291	$\frac{17}{2}^+ \rightarrow \frac{13}{2}^+$	$\sigma(\frac{17}{2}^+) = 1.75 \pm 0.30$
884.6 ± 0.5	8		0.41 ± 0.06	−0.02 ± 0.07	4352 → 3467	$(\frac{21}{2}^-) \rightarrow \frac{21}{2}^+$	$\sigma(\frac{21}{2}^-) = 3.0 \pm 0.7$
1082.6 ± 0.5	Doublet [e]	Doublet [e] ~1 [d]			1187 → 104	$\frac{5}{2}^- \rightarrow \frac{1}{2}^-$	
1208 ± 1	13		−0.05 ± 0.07	0.04 ± 0.08	1313 → 104	$\frac{3}{2}^- \rightarrow \frac{1}{2}^-$	
1581 ± 1	~10				1581 → 0	$\frac{7}{2}^+ \rightarrow \frac{9}{2}^+$	
1637 ± 1	~10				1637 → 0	$\frac{9}{2}^+ \rightarrow \frac{9}{2}^+$	
1715 ± 2	Doublet				5182 → 3467	$(\frac{23}{2}, \frac{25}{2}) \rightarrow \frac{21}{2}^+$	
1790.6 ± 0.5	58	33.5 ± 1.0 [c]	0.18 ± 0.02	0.06 ± 0.03	1791 → 0	$\frac{9}{2}^- \rightarrow \frac{9}{2}^+$	
1984.6 ± 0.5	93	57.7 ± 1.0 [c]	0.12 ± 0.02	−0.06 ± 0.02 [f]	1985 → 0	$\frac{13}{2}^- \rightarrow \frac{9}{2}^+$	$\delta(E3/M2) = -10 \pm 4$ or $\delta(E3/M2) = -0.11 \pm 0.06$
2062.1 ± 0.5	26		−0.15 ± 0.08	−0.09 ± 0.09	4097 → 2035	$(\frac{19}{2}^-) \rightarrow \frac{17}{2}^-$	
2290.9 ± 0.5	100		0.35 ± 0.03	−0.09 ± 0.03	2291 → 0	$\frac{13}{2}^+ \rightarrow \frac{9}{2}^+$	$\sigma(\frac{13}{2}^+) = 1.95 \pm 0.25$
2414 ± 1	10		−0.17 ± 0.11	−0.03 ± 0.13	2414 → 0	$\frac{11}{2}^- \rightarrow \frac{9}{2}^+$	

[a] The intensities have about a 10% over-all uncertainty which includes the efficiency correction uncertainty. Branching ratios shown in Fig. 6 sometimes have a smaller uncertainty when they can be determined from γ rays with similar energies.

[b] Given here are attenuation coefficients α_k, the width $\sigma(J)$ for an assumed Gaussian m-substate distribution, and the $E(L+1)/M(L)$ mixing ratio δ.

[c] Intensity integrated over 0°, 45°, and 90°.

[d] Intensity at 90°.

[e] A 1083-keV γ ray also originates from the ^{88}Zr $4^+ \rightarrow 2^+$ transition which contains a $\tau = 2.5$-μsec delayed component. [M. Ishihara, H. Kawakami, N. Yoshikawa, M. Sakai, and K. Ishii, Phys. Lett. 35B, 398 (1971)].

[f] $A_6 = 0.00 \pm 0.03$.

TABLE III. Properties of γ rays assigned to transitions in ^{91}Zr from the ^{88}Sr(^{6}Li, $p2n$) ^{91}Zr reaction.

E_γ (keV)	Isomeric intensity[a] (Relative units)	A_2[b]	A_4	Transition assignment $E_i \rightarrow E_f$ (keV) (keV)	$J_i^\pi \rightarrow J_f^\pi$
28.0± 0.2	···			2287 → 2259	$\frac{15}{2}^- \rightarrow \frac{13}{2}^-$
38.7± 0.2	···			2170 → 2131	$\frac{11}{2}^- \rightarrow \frac{9}{2}^+$
60.3± 0.2	···			2320 → 2260	$\frac{11}{2}^- \rightarrow \frac{13}{2}^-$
89.5± 0.2	···			2259 → 2170	$\frac{13}{2}^- \rightarrow \frac{11}{2}^-$
150 ± 1	Weak			2320 → 2170	$\frac{11}{2}^- \rightarrow \frac{11}{2}^-$
289.8± 0.3	13[c]	0.26± 0.07	−0.26± 0.10	3146 → 2857	$\frac{17}{2}^+ \rightarrow \frac{13}{2}^+$
477 ± 1		−0.25± 0.16	0.11± 0.20	2764 → 2288	$(\frac{13}{2}^-) \rightarrow \frac{15}{2}^-$
537 ± 1	1.7[c]			2857 → 2320	$\frac{13}{2}^+ \rightarrow \frac{11}{2}^-$
570 ± 1	1.3[c]			2857 → 2288	$\frac{13}{2}^+ \rightarrow \frac{15}{2}^-$
596.9± 0.3	3.9[c]			2857 → 2260	$\frac{13}{2}^+ \rightarrow \frac{13}{2}^-$
725.7± 0.3	6.4[c]	0.21± 0.08	−0.19± 0.10	2857 → 2131	$\frac{13}{2}^+ \rightarrow \frac{9}{2}^+$
859.0± 0.3	98[d]	−0.13± 0.03	−0.04± 0.03	3146 → 2287	$\frac{17}{2}^+ \rightarrow \frac{15}{2}^-$
879.4± 0.3	4.4[c]			3167 → 2287	$\frac{21}{2}^+ \rightarrow \frac{15}{2}^-$
2131.1± 0.5	16[d]			2131 → 0	$\frac{9}{2}^+ \rightarrow \frac{5}{2}^+$
2169.9± 0.5	100[d]	0.44± 0.03	0.01± 0.03[e]	2170 → 0	$\frac{11}{2}^- \rightarrow \frac{5}{2}^+$

[a] Intensities have about a 10% uncertainty. (See footnote a in Table II.)
[b] Singles angular distribution.
[c] Intensity at 90°. The angular distribution correction is small due to attenuation.
[d] Intensity integrated over 0°, 45°, and 90°.
[e] $A_6 = -0.03 \pm 0.03$.

keV which is actually required for the $\frac{11}{2}^- \rightarrow \frac{9}{2}^-$ transition) was not in coincidence with the 1791-keV γ ray. The 2661-keV → 2035-keV transition of 626 keV was not seen in coincidence with γ rays originating below the $\tau = 5.42$ μsec 2035-keV $\frac{17}{2}^-$ level because of the resolving time of about 200 nsec used for the γ-γ coincidence.

No 1076-keV γ ray, required for a decay branch from the 3110-keV $\frac{17}{2}^+$ level to the 2035-keV $\frac{17}{2}^-$ level, was observed in coincidence with the 357-keV γ ray. A weak 1077-keV γ ray observed in the singles spectrum is probably mostly due to Coulomb excitation of the ^{86}Sr 2^+ state. The singles intensity of the 450- and 819-keV γ rays gives a (9 ± 2)% branch for the $\frac{17}{2}^+ \rightarrow (\frac{15}{2}^-, \frac{19}{2}^-)$ transition assuming no $\frac{17}{2}^+ \rightarrow \frac{17}{2}^-$ branch. An upper limit of 8% can be set for the $\frac{17}{2}^+ \rightarrow \frac{17}{2}^-$ branch.

The 885-keV γ ray is the strongest γ ray in coincidence with the 357-keV transition and thus must feed the 3467-keV level. The 885-keV γ ray together with the sum of the energies of the 254- and 2062-keV γ rays, which are in strong coincidence with each other, indicates a level at 4352 keV with a 38% branch to the $\frac{21}{2}^+$ level and a 62% branch, via the 254-2062-keV cascade, to the $\frac{17}{2}^-$ level. From the singles intensities, the intermediate state in the cascade is at 4097 keV. The angular distribution of the 885-keV transition ($A_2 > 0, A_4 \approx 0$) is characteristic of a $J \rightarrow J$ $l = 1$ transition (a $J \rightarrow J - 2$ $l = 2$ transition would have $A_2 > -A_4 > 0$). The angular distributions of the 254- and 2062-keV γ rays are characteristic of $J \rightarrow J - 1$ $l = 1$ transitions with small $l = 2$ admixtures ($M1 + E2$ transitions). All of this information suggests spin and parity assignments of $\frac{21}{2}^-$ and $\frac{19}{2}^-$ for the 4352 and 4097-keV levels, respectively.

A weak 1715-keV γ ray was also in coincidence with the 357-keV transition which is very likely due to feeding of the $\frac{21}{2}^+$ level from a level at 5182 keV. The angular distribution for the 1715-keV γ ray could not be obtained due to a contaminant γ ray of uncertain origin with about the same energy in the singles spectra. A spin of $\frac{23}{2}$ or $\frac{25}{2}$ for the 5182-keV level is suggested by yrast arguments.

A number of weaker γ rays were observed in coincidence with the γ rays discussed above (see Table I); the primary ones are: 186 (doublet),

258, 421, 497, 817, 919, and 1014 keV. Because of the similarity in the intensities of a number of these γ rays, they could not unambiguously be incorporated into the ^{91}Nb level scheme. Most of these γ rays probably feed the 4352-keV level; the strongest (186, 421, and 919 keV) have negative A_2 coefficients.

C. ^{91}Nb mixing ratios

Mixing ratios have been obtained for three transitions in ^{91}Nb using the spin assignments discussed in the last section. The dependence on the m-substate distribution was obtained from an analysis of the strongest pure multipolarity ($\delta = 0$) $E1$ and $E2$ transitions assuming the Gaussian m-substate distribution discussed in Sec. IIC. An average value for the Gaussian width of $\sigma = 2.0 \pm 0.3$ was obtained from this analysis (see Table II) and was subsequently used to obtain the mixing ratios for the other prompt transitions.

A mixing ratio of $\delta(E2/M1) = -0.42 \pm 0.05$ was obtained for the 430-keV γ ray which has been assigned to the 2414-keV $\frac{11}{2}^- \rightarrow$ 1985-keV $\frac{13}{2}^-$ transition. For the 626-keV γ ray assigned to the 2661-keV $J_i \rightarrow$ 2035-keV $\frac{17}{2}^-$ transition, equally acceptable fits were obtained for the two choices of initial spins; $\delta(E2/M1) = -0.02 \pm 0.05$ for $J_i = \frac{15}{2}$ and $\delta(E2/M1) = 0.06 \pm 0.06$ for $J_i = \frac{19}{2}$. The mixing ratio for the 430-keV γ ray is in agreement with another recent determination by Berinde *et al.*[21] However, the present result for the 626-keV γ ray is different from Berinde *et al.* because of a different assumed transition assignment as well as the fact that the experimental angular distribution coefficients are in disagreement.

The $E3/M2$ mixing ratio of the 1985-keV γ ray was also obtained. This transition cannot be handled as simply as the prompt transitions (with an assumed Gaussian m-substate distribution) because about 65% of the 1985-keV γ ray is delayed by the $\tau = 5.42$ μsec isomer from which some, although not complete, attenuation takes place. In this case the attenuation (α_2 and α_4) of the complete-alignment angular distributions coefficients,

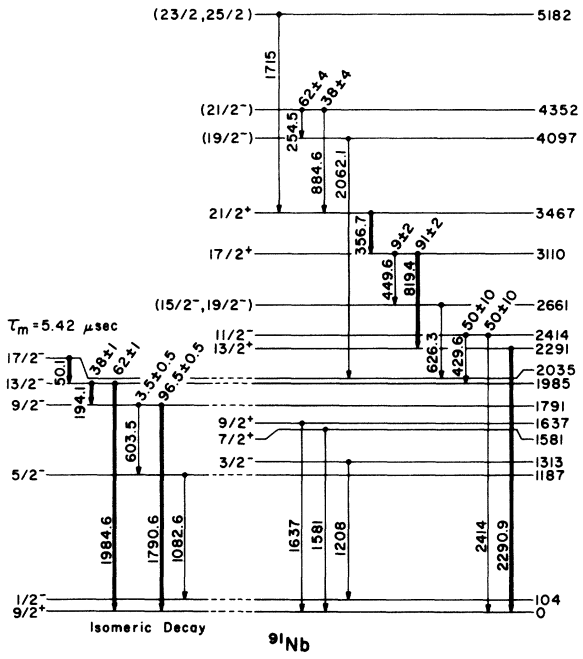

FIG. 6. The decay scheme for ^{91}Nb from the present work. The transitions involved in the decay of the $\tau = 5.42 \pm 0.18$ μsec $\frac{17}{2}^-$ isomeric state are shown on the left. The intensified transitions indicate the dominant decay modes of levels most strongly populated in the ^{88}Sr(^{6}Li, 3n) ^{91}Nb reaction. The spin assignments for levels below 1791 keV are taken from Refs. 17–19.

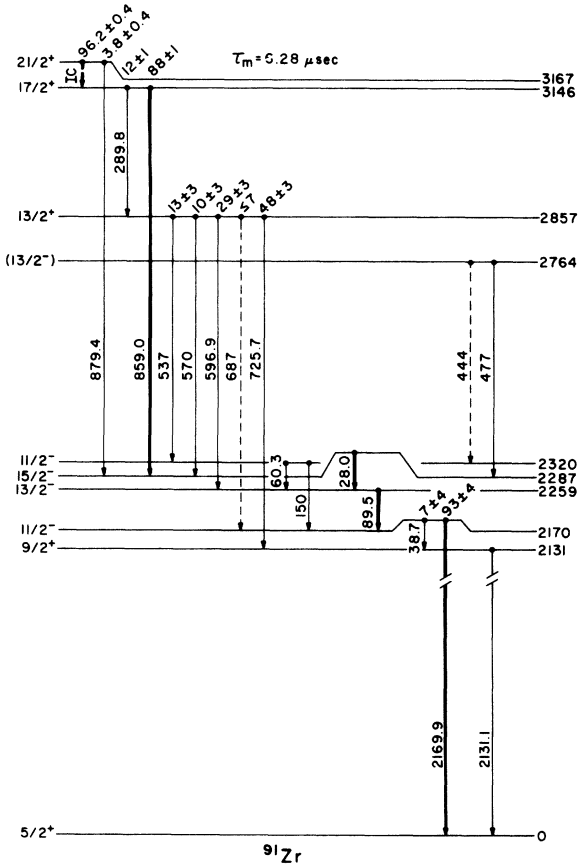

FIG. 7. The decay scheme for ^{91}Zr from the present work. The intensified transitions indicate the dominant decay modes of levels most strongly populated in the ^{88}Sr(^{6}Li,$p2n$)^{91}Zr reaction. The $\frac{21}{2}^+ \rightarrow \frac{17}{2}^+$ isomeric transition labeled IC was deduced as internal conversion by the subsequent delayed cascade γ rays and its energy determined from the weak 879.4-keV decay branch.

was taken from the 194-keV $E2$ branch of the 1985-keV $\frac{13}{2}^-$ level (see Table II). The α_6 attenuation coefficient was then estimated by assuming an m-substate population for the $\frac{13}{2}^-$ level given by a sum of two Gaussians. Two acceptable fits were obtained for the mixing ratio: $\delta(E3/M2) = -10 \pm 4$ or $\delta(E3/M2) = -0.11 \pm 0.06$. The errors include the uncertainties in α_k.

D. ^{91}Zr isomeric and prompt decay

In ^{91}Zr an isomeric $\frac{21}{2}^+$ state at 3167 keV with a mean lifetime of $\tau = 6.28 \pm 0.20$ μsec was found. Nearly all of the other high-spin levels observed in ^{91}Zr are fed to some extent by the isomeric decay. The ^{91}Zr decay scheme from the present experiment is shown in Fig. 7 and the γ-ray properties are summarized in Table III. Previous results, which are most important for the present discussion related to the high-spin levels, were obtained from ^{88}Sr$(\alpha, n)^{91}$Zr experiments[20,25] and the high resolution ^{91}Zr$(p, p')^{91}$Zr experiment of Blok.[22]

The 90-, 2170-, and 859-keV γ rays were in strong coincidence from the Ge(Li) γ-γ data and appeared in the μsec-delayed region (see Fig. 2) yielding a consistent mean lifetime that averaged $\tau = 6.28 \pm 0.20$ μsec. The 90- and 2170-keV γ rays also contained a shorter component ($\tau \simeq 50$ nsec). Previously, with the reaction ^{88}Sr$(\alpha, n)^{91}$Zr, these two γ rays were assigned to the $\frac{13}{2}^- \rightarrow \frac{11}{2}^- \rightarrow \frac{5}{2}^+$ cascade and measured to have a time dependence of $\tau = 41.8 \pm 1.2$ nsec which was attributed to an unobserved $\frac{15}{2}^- \rightarrow \frac{13}{2}^-$ cascade with $E_\gamma < 80$ keV.[20] In the present experiment, a 28.0 ± 0.1-keV γ ray was found to be in coincidence with the high-energy γ rays, by a Si(Li)-Ge(Li) detector combination, and it displayed the same μsec time dependence (see Fig. 4). The 28-keV γ ray has been assigned to a 2287-keV $\frac{15}{2}^- \rightarrow$ 2259-keV $\frac{13}{2}^-$ $M1$ transition on the basis of the γ-γ data, the I_γ (ICC = 8.0), the lifetime, and the precise energy agreement with levels observed with $L = 5$ in the (p, p') experiment of Blok.[22] The delay observed between the 28 and 859-keV γ rays in the Si(Li)-Ge(Li) coincidence is consistent with the mean lifetime ($\tau = 41.8$ nsec) attributed to the 2287-keV $\frac{15}{2}^-$ level.

The 859-keV γ ray, which thus originates from a level at 3146 keV, contained a 35% prompt component which means that the μsec isomer must originate from an unobserved low-energy γ ray ($E_\gamma \leq 36$ keV) feeding this level, most likely a highly converted $E2$ transition. The coincident triplet of weaker γ rays, 290, 726, and 2131 keV which also appears in the delayed spectra represents a 12% branch of the 3146-keV level to the previously known 2131-keV $\frac{9}{2}^+$ level[25] via an intermediate state at 2857 keV. The angular distributions and prompt lifetime limits ($\tau \leq 10$ nsec) observed for the 290-, 726-, and 859-keV γ rays (see Table III) strongly suggest spin assignments of $\frac{17}{2}^+$ for the 3146-keV level and $\frac{13}{2}^+$ for the 2857-keV level.

Several less intense γ rays were observed in the μsec-delayed spectra with delayed components of about 6 μsec (see Fig. 3). Three of these (537, 570, and 597 keV) represent $E1$ decay branches of the 2857-keV $\frac{13}{2}^+$ level to the known negative-parity states near 2.3 MeV. A higher-energy 879-keV γ ray must originate from a branch (3.8%) of the $\tau = 6.28$ μsec isomeric state to the 2287-keV $\frac{15}{2}^-$ level. The strength for this transition is consistent with the $E3$ strength observed for the $8^+ \rightarrow 5^-$ transition in ^{90}Zr.[31,32] Thus the isomeric state in ^{91}Zr is located at 3167 keV with a spin of $\frac{21}{2}^+$ and it decays with a 96.2% branch to the $\frac{17}{2}^+$ state via internal conversion (ICC = 316). The precise energy difference of the 879- and 859-keV γ rays was measured to be 20.4 ± 0.2 keV.

Every level observed in the present experiment is in remarkable agreement with levels found in the high resolution (p, p') ($E_p = 20.47$ MeV) experiment of Blok.[22] An additional weak 477-keV γ ray observed in coincidence with the 90-keV transition has been assigned to the 2764-keV $\rightarrow$ 2287-keV $\frac{15}{2}^-$ transition on the basis of a level observed at 2766 keV with $L = 5$ in the (p, p') experiment. An unassigned 444-keV γ ray reported by Glenn, Baer, and Kraushaar[25] could possibly be the 2764-keV $\rightarrow$ 2320-keV $\frac{11}{2}^-$ transition, but this cannot be confirmed in the present experiment because of a strong contaminant 442-keV γ ray from ^{88}Y. On the basis of the decay mode for the 2764-keV level and its appearance with $L = 5$ in the (p, p') experiment, the most likely spin assignment is $\frac{13}{2}^-$.

Finally, several other low energy γ rays can be associated with ^{91}Zr. A 60-keV γ ray was observed in coincidence with the 2170-keV transition. In the (α, n) experiment of Glenn *et al.*,[25] 61- and 151-keV γ rays were associated with the decay of the 2320-keV $\frac{11}{2}^-$ level. This would be consistent with the coincidence result, but the 2320-keV level is populated too weakly in the present experiment to obtain further information. A 39-keV γ ray which was in coincidence with the 2131-keV transition is due to a 2170-keV $\frac{11}{2}^- \rightarrow$ 2131-keV $\frac{9}{2}^+$ $E1$ transition. A $\frac{11}{2}^- \rightarrow \frac{9}{2}^+$ branching ratio of $(7 \pm 4)\%$ was determined from the intensity balance of the delayed transitions.

IV. DISCUSSION

In the following sections the experimental level properties of ^{91}Nb and ^{91}Zr are discussed in terms

of a shell-model basis which includes the $2p_{1/2}$ and $1g_{9/2}$ orbitals for protons and the $2d_{5/2}$ and $3s_{1/2}$ orbitals for neutrons outside of an ^{88}Sr closed core. The theoretical energy levels and electromagnetic matrix elements were obtained from a recent study of the mass-90 region by Gloeckner *et al.*[10-12] In this study the effective interactions were obtained from a least-squares fit to many $N=50$ and $N=51$ energy levels, including ^{91}Nb and ^{91}Zr levels, assuming unrestricted two-body interaction matrix elements. For the $N=50$ nuclei the proton-proton interaction was found to be nearly seniority conserving; the seniority-conserving interaction, given in column 3 of Table 2 in Ref. 11, was used for the present comparison. The neutron-proton interaction used for ^{91}Zr and other $N=51$ nuclei is given in column 3 of Table 2 in Ref. 12.

Within this model space, the ^{91}Nb positive-parity states are described by $g_{9/2}(p_{1/2})^2$ and $(g_{9/2})^3$ configurations and the negative-parity states by $(g_{9/2})^2p_{1/2}$ configurations. The ^{91}Zr positive-parity states consist of the $d_{5/2}$ and $s_{1/2}$ neutrons coupled to the ^{90}Zr $(p_{1/2})^2$ and $(g_{9/2})^2$ configurations and the negative-parity states result from the coupling of these neutrons to the ^{90}Zr $g_{9/2}p_{1/2}$ configurations.

Other states based on the ^{88}Sr core excitations which are outside the model space are expected. They include the low-lying 3^- and 2^+ vibrational states found in most spherical nuclei. Possible multiplets involving the ^{90}Zr 3^- state in ^{91}Nb and ^{91}Zr will be discussed.

Effective two-body interaction and one-body electromagnetic operators have been introduced to account for the small admixtures of the ^{88}Sr core excitations into the model space wave functions.[33] In the discussion below, emphasis has been placed on the relatively straightforward interpretation which is possible for the effective electromagnetic operators, in particular for the electric quadrupole ($E2$) operator. The $E2$ effective charge, which represents the enhancement of the $E2$ matrix elements, will be discussed for the mass-90 region in terms of its dependence on the nuclear states involved. In addition, a brief comparison with other mass regions, based on average effective charges, will be presented.

A. ^{91}Nb and $N=50$ energy levels

The theoretical energy levels[11] for ^{91}Nb are compared with the results from the present and previous experiments in Fig. 8. All of the theoretical positive-parity states from the configuration $(g_{9/2})^3$ except for the $\frac{15}{2}^+$ state can be tentatively associated with observed levels. The $\frac{9}{2}^+$ ground-state is predominantly $g_{9/2}(p_{1/2})^2$ or written simply $g_{9/2}$. The $\frac{21}{2}^+$, $\frac{17}{2}^+$, $\frac{13}{2}^+$, and two lowest $\frac{9}{2}^+$ states were included in Gloeckner's least-squares fit for the $N=50$ nuclei. Hence, the good theoretical agreement for these levels means that a consistent interpretation for them together with other $N=50$ high-spin levels is possible within the small $g_{9/2}$-$p_{1/2}$ model space. The other levels which were not included in the least-squares fit can thus be considered true predictions of the theoretical calculation. The theoretical-experimental deviations are a little worse for these low-spin states compared with the high-spin states, but the over-all agreement is still very good.

The experimental 2580-keV $\frac{5}{2}^+$ and 2793-keV $\frac{7}{2}^+$ levels may be the weak-coupling doublet expected

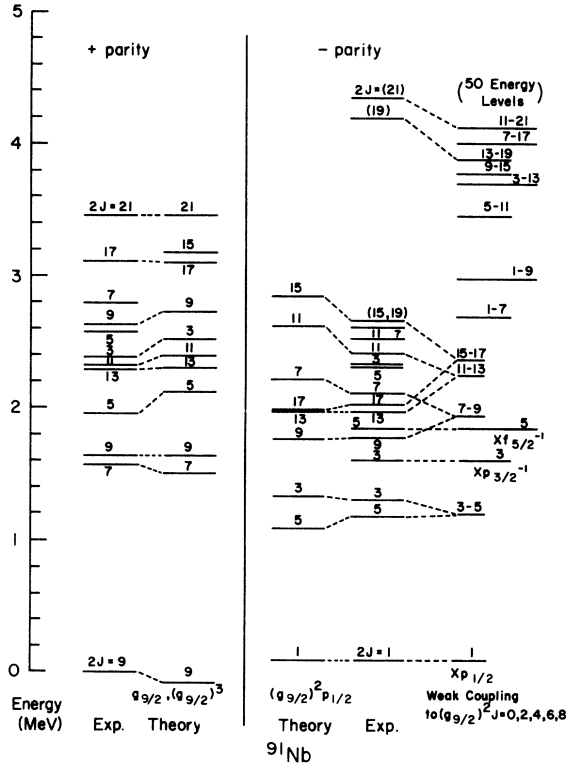

FIG. 8. Comparison of experimental and theoretical energy levels for ^{91}Nb. The spins are indicated by $2J$. The experimental information is from the present work and from Refs. 17–19. The theoretical energy levels marked theory are the results of the "total energy" fit of Gloeckner *et al.* (Ref. 11). The total energy fit results for the proton-proton interaction are nearly identical to the seniority conserving interaction obtained by Gloeckner *et al.* (Ref. 11) which is discussed in the text (Sec. IV). The centroids of the weak coupling multiplets which we evaluated for the $(g_{9/2})^2p_{1/2}$ and $(g_{9/2})^2(p_{1/2})^2j^{-1}$ configurations where $j^{-1}=p_{3/2}{}^{-1}$ or $f_{5/2}{}^{-1}$ are shown on the extreme right side. The notation "1–7," for example, indicates the multiplet $\frac{1}{2}^-$, $\frac{3}{2}^-$, $\frac{5}{2}^-$, and $\frac{7}{2}^-$.

TABLE IV. $B(E2)$ values for $N=50$ nuclei.

Nucleus	$J_i \to J_f$	$\tau(J_i)$	E_γ (keV)	Branching ratio (%)	ICC [a]	$B(E2)_{exp}$ [b] (e^2 fm^4)	Proton configuration	$B(E2)_{th}$ [c,d] ($e_p{}^2$ fm^4)	e_p [e] (e)
^{90}Zr	$8^+ \to 6^+$	180 ± 7 nsec [f]	141.1 [g]	98 [g]	0.318	60.5 ± 2.5	$g_{9/2}{}^2$	16.5	1.91 ± 0.05
	$6^+ \to 4^+$						$g_{9/2}{}^2$	41.3	
	$4^+ \to 2^+$						$g_{9/2}{}^2$	59.7	
	$2^+ \to 0^+$					285 ± 25 [h]	$g_{9/2}{}^2$	52.0	2.18 ± 0.10
^{91}Nb	$\frac{21}{2}^+ \to \frac{17}{2}^+$	1.33 ± 0.14 nsec [i]	357	100	0.012	106 ± 11	$g_{9/2}{}^3$	33.1	1.79 ± 0.09
	$\frac{17}{2}^+ \to \frac{13}{2}^+$						$g_{9/2}{}^3$	57.7	
	$\frac{17}{2}^- \to \frac{13}{2}^-$	5.42 ± 0.18 μsec [j]	50.1 [j]	100	13.9	32.0 ± 1.9	$g_{9/2}{}^2 p_{1/2}$	16.5	1.39 ± 0.04
	$\frac{13}{2}^- \to \frac{9}{2}^-$	14.4 ± 0.5 nsec [k]	194.1 [j]	38 ± 1 [j]	0.103	71.1 ± 3.2	$g_{9/2}{}^2 p_{1/2}$	41.3	1.31 ± 0.03
	$\frac{9}{2}^- \to \frac{5}{2}^-$	≥2.3 psec [l]	603	3.5 ± 0.5 [j]		≤178	$g_{9/2}{}^2 p_{1/2}$	59.7	≤1.7
^{92}Mo	$8^+ \to 6^+$	275 ± 10 nsec [m]	148	100	0.29	32.4 ± 1.2	$g_{9/2}{}^2 p_{1/2}{}^2 + g_{9/2}{}^4$	12.2*	<u>1.63 ± 0.03</u>
	$6^+ \to 4^+$	2.22 ± 0.07 nsec [m]	330	85 [m]	0.017	78.5 ± 2.5	$g_{9/2}{}^2 p_{1/2}{}^2 + g_{9/2}{}^4$	30.5*	<u>1.60 ± 0.03</u>
	$2^+ \to 0^+$					234 ± 40 [n]	$g_{9/2}{}^2 p_{1/2}{}^2 + g_{9/2}{}^4$	57*	2.26 ± 0.19
	$11^- \to 9^-$	12.7 ± 0.7 nsec [o]	235	100	0.05	85 ± 5	$g_{9/2}{}^3 p_{1/2}$	33.1	1.60 ± 0.04
^{93}Tc	$\frac{21}{2}^+ \to \frac{17}{2}^+$	2.32 ± 0.14 nsec [i]	350	100	0.015	65.9 ± 4.0	$g_{9/2}{}^3 p_{1/2}{}^2 + g_{9/2}{}^5$	24.3*	<u>1.69 ± 0.05</u>
	$\frac{17}{2}^- \to \frac{13}{2}^-$	15.2 ± 1.0 μsec [p]	39.75 [p]	73.7 [p]	34.1	11.4 ± 0.9	$g_{9/2}{}^4 p_{1/2}$	1.84	2.49 ± 0.10
^{94}Ru	$8^+ \to 6^+$	102 ± 7 μsec [o]	145	100	0.33	$(9.4 \pm 0.6) \times 10^{-2}$	$g_{9/2}{}^4 p_{1/2}{}^2 + g_{9/2}{}^6$	0.75*	0.35 ± 0.01
	$6^+ \to 4^+$	107 ± 10 nsec [o]	311	100	0.024	2.56 ± 0.24	$g_{9/2}{}^4 p_{1/2}{}^2 + g_{9/2}{}^6$	1.87*	1.17 ± 0.05
								Average [q]	1.63 ± 0.03

[a] The internal conversion coefficients were interpolated from the tables of Hager and Seltzer (Ref. 30). An uncertainty of 5% for the ICC was assumed.

[b] $B(E2)_{exp} = 0.816$ (branching ratio/100)/$[E_\gamma{}^5$(MeV)(1 + ICC)τ(nsec)].

[c] The theoretical $B(E2)$ values are calculated for wave functions with good seniority. The values marked with an asterisk for cases with the two configurations, $g_{9/2}^n p_{1/2}{}^2$ and $g_{9/2}^{n+2}$, were obtained by Gloeckner *et al.* (Refs. 10, 11, and 40).

[d] $\langle g_{9/2} | r^2 | g_{9/2} \rangle = 26.0$ fm^2 ($\nu = 0.212$).

[e] $e_p = [B(E2)_{exp}/B(E2)_{th}]^{1/2}$.

[f] Reference 32.

[g] H. Pettersson, S. Antman, and Y. Grunditz, Nucl. Phys. <u>A108</u>, 124 (1968).

[h] Sum of the $B(E2)$ values for the ^{90}Zr $2_1^+ \to 0_1^+$ and $2_1^+ \to 0_2^+$ transitions. $B(E2, 2_1 \to 0_1) = 135 \pm 12$ e^2 fm^4 and $B(E2, 2_1 \to 0_2)/B(E2, 2_1 \to 0_1) = 1.11$ (Ref. 31).

[i] Reference 35.

[j] Present experiment.

[k] Reference 20.

[l] Reference 17.

[m] Reference 37.

[n] P. H. Stelson and L. Grodzins, Nucl. Data <u>A1</u>, 21 (1965).

[o] Reference 6.

[p] Reference 16.

[q] This average only considers the three values underlined for which the $2p_{1/2}$ shell is mostly filled.

at this excitation energy from the $(^{90}\mathrm{Zr}\ 3^-)\otimes p_{1/2}$ configuration. The $2J+1$ weighted energy average for these two states gives 2.702 MeV for the centroid which is in good agreement with the ^{90}Zr 3^- level at 2.748 MeV.[31]

The negative-parity states in ^{91}Nb from the $(g_{9/2})^2 p_{1/2}$ configurations are particularly simple to understand. They form a series of doublets with the configuration $[(g_{9/2})^n J_0, p_{1/2}]J$ where $J = J_0 \pm \frac{1}{2}$, and $J_0 = 0$, 2, 4, 6, and 8 with $n = 2$. The energies of these states are given by[4,34]

$$C_p + nC_g + V(J_0) + n\alpha + [J(J+1) - J_0(J_0+1) - \tfrac{3}{4}]\beta,$$

where C_p and C_g are the single-particle energies and $V(J_0)$ is the interaction energy of the state $(g_{9/2})^n J_0$. The α and β coefficients are defined as $\alpha \equiv \frac{1}{2}[0.9\,V(4^-) + 1.1\,V(5^-)]$ and $\beta \equiv \frac{1}{10}[V(5^-) - V(4^-)]$, where $V(4^-)$ and $V(5^-)$ are the interaction energies for the configurations $(g_{9/2}p_{1/2})$ $(J = 4^-, 5^-)$. The energy difference between the members of the multiplet $J = J_0 \pm \frac{1}{2}$ is given simply by $(2J_0+1)\beta$. The values of $\beta = 0.025$–0.037 deduced for these ^{91}Nb negative-parity doublets are smaller than the average value $\beta = 0.052$ obtained from the theoretical $N = 50$ least-squares fit. This discrepancy which, in particular, includes a somewhat poorer agreement for the $\frac{11}{2}^-$ and $\frac{15}{2}^-$ levels in ^{91}Nb may be due to perturbations from the other expected negative-parity states discussed below.

In order to explain the 1613-keV $\frac{3}{2}^-$ and 1845-keV $\frac{5}{2}^-$ levels, multiplet configurations involving holes (j^{-1}) in the $2p_{3/2}$ and $1f_{5/2}$ orbitals of the form

$$[(g_{9/2})^2 J_0, (p_{1/2})^2 j^{-1}]J$$

have to be introduced. The largest component for the $\frac{3}{2}^-$ and $\frac{5}{2}^-$ states is expected to have $J_0 = 0$. The centroids of these multiplets which we evaluated in an extreme weak-coupling model for all values of J_0 are shown on the right-hand side of Fig. 8. The highest-spin states of $\frac{19}{2}^-$ and $\frac{21}{2}^-$, expected at about 4 MeV in excitation, are in fairly good agreement with the experimentally observed high-spin states at about this energy.

In addition to the negative-parity levels discussed above, a negative-parity multiplet with spins $\frac{3}{2}^-$ to $\frac{15}{2}^-$ is expected at about 2.75 MeV from the $(^{90}\mathrm{Zr}\ 3^-)\otimes g_{9/2}$ configuration. In the weak-coupling model the $E3$ decay for each of these states to the ^{91}Nb ground state has the same enhanced $B(E3)$ value as that observed for the $^{90}\mathrm{Zr}\ 3^- \rightarrow$ g.s. transition,[31] $B(E3\downarrow) = (15.4 \pm 0.4) \times 10^3\ e^2\,\mathrm{fm}^6 = 32$ W.u. (Weisskopf units). From the lifetime and branching ratio for the 1985-keV $\frac{13}{2}^-$ level, an upper limit of $B(E3) \leq 650\ e^2\,\mathrm{fm}^6 = 1.3$ W.u. is obtained for the $\frac{13}{2}^- \rightarrow \frac{9}{2}^+$ $E3/M2$ transition which implies that this $\frac{13}{2}^-$ level can have at most a 4% admixture of the $\frac{13}{2}^-$ member of the collective multiplet. This collective multiplet has not been identified experimentally. The levels at 2414 and 2532 keV have both been assigned $\frac{11}{2}^-$.[18] Only the lowest level has a branch to the 1985-keV $\frac{13}{2}^-$ level which suggests that this level is predominantly the $\frac{11}{2}^-$ member of the $[(g_{9/2})^2 6^+, p_{1/2}]$ multiplet discussed above, while the upper $\frac{11}{2}^-$ level is part of the collective 3^- multiplet.

B. ^{91}Nb and $N = 50$ $B(E2)$ values

With the results of the present experiment together with other recent lifetime measurements,[20,35] accurate values for the reduced $E2$ transition probabilities for three transitions between high-spin states in ^{91}Nb are deduced. These $B(E2)$ values together with $B(E2)$ values deduced for states of the $g_{9/2}$-$p_{1/2}$ configurations in the other $N = 50$ nuclei are summarized in Table IV.

Within the $g_{9/2}$-$p_{1/2}$ model space, the theoretical $B(E2)$ values are straightforward to calculate.[35] For most of the matrix elements in ^{90}Zr and ^{91}Nb, the theoretical $E2$ matrix elements are uniquely determined, and thus the effective $E2$ operator can be deduced independent of any assumptions regarding the two-body matrix elements. Furthermore, with the assumption used for Table IV, that no seniority mixing occurs, all of the $B(E2)$ values for transitions between the $N = 50$ negative-parity states are similarly unique.

The matrix elements discussed above are all proportional to the $\langle g_{9/2} \| r^2 Y^{(2)} e_p \| g_{9/2} \rangle$ reduced single-particle matrix element. The r^2 radial matrix elements are calculated in the harmonic oscillator model using an oscillator parameter $(\nu = m\omega/\hbar)$ which is required to reproduce the root-mean-square (rms) radius of ^{90}Zr deduced from electron scattering data. The rms radius of ^{90}Zr is 4.27 fm[36] which after correction for the finite proton rms radius of 0.64 fm[36] gives a value $\nu = 0.212$ and $\langle g_{9/2} | r^2 | g_{9/2} \rangle = 26.0\ \mathrm{fm}^2$. This is the same $\langle r^2 \rangle$ value which has been recently used by Gloeckner *et al.*[10–12] (Other slightly different values for the $\langle r^2 \rangle$ matrix element have been used in previous discussions[35,37] including our own preliminary reports[14,15] which lead to small changes in the deduced effective charges.)

The proton effective charges extracted from the comparison of experimental and theoretical $B(E2)$ values are given in Table IV. The comparison between different nuclei and even between transitions within a given nucleus shows considerably more variation in the proton effective charges than has been obtained from similar straightforward comparisons for the $N = 28$ nuclei[38] and the $N = 126$ nuclei.[39]

For ^{94}Ru the agreement can be significantly im-

TABLE V. Comparison of theoretical and experimental $E2/M1$ mixing ratios between the negative parity doublets in ^{91}Nb.

J_0	$J_i \to J_f$	$Q(J_0)_{\rm th}$ [a] (e fm^2)	E_γ(exp) (MeV)	$\delta(E2/M1)_{\rm th}$ [b]	$\delta(E2/M1)_{\rm exp}$
8^+	$\frac{15}{2}^- \to \frac{17}{2}^-$	34.0	0.626	−0.017	−0.02 ± 0.05
6^+	$\frac{11}{2}^- \to \frac{13}{2}^-$	6.8	0.430	−0.003	−0.42 ± 0.05
4^+	$\frac{7}{2}^- \to \frac{9}{2}^-$	−10.8	0.330	0.006	
2^+	$\frac{3}{2}^- \to \frac{5}{2}^-$	−17.0	(0.126) [c]	0.009	

[a] $e_p = 1.35$
[b] $g(g_{9/2}) = 1.36$ (Ref. 31) and $g(p_{1/2}) = -0.27$ (Ref. 41).
[c] Transition has not been observed experimentally.

proved by introducing small seniority mixing.[11] It has also been shown that the ^{93}Tc $\frac{17}{2}^- \to \frac{13}{2}^-$ transition matrix element is sensitive to seniority mixing.[40] These particular $E2$ matrix elements show this seniority sensitivity because of the large values of the $\Delta\nu = 2$ $E2$ matrix elements compared with the relatively small $\Delta\nu = 0$ $E2$ matrix elements in the middle of the $g_{9/2}$ shell. In addition, because the $\Delta\nu = 0$ pure seniority matrix elements are small in these cases, contributions other than seniority mixing, such as those discussed in the next paragraph, may be important.

The variations in the effective charge for the transitions that are unique within the $g_{9/2}$-$p_{1/2}$ configuration are probably due to the exclusion of the $1f_{5/2}$ and $2p_{3/2}$ protons from the model space whose virtual excitations to the $2p_{1/2}$ orbital will enter linearly into the $E2$ matrix elements. The effect of these virtual excitations may be different for the high-spin positive-parity states in ^{90}Zr and ^{91}Nb where the $2p_{1/2}$ orbital is empty than for the negative-parity states in ^{91}Nb where the $2p_{1/2}$ orbital is half full.

The most unambiguous value for the $1g_{9/2}$ proton effective charge can thus be obtained from the $E2$ transitions in Table IV which have a dominant configuration of the type $(1g_{9/2})^n(2p_{1/2})^2$ and have large $B(E2)$ values. Considering only the transitions ^{92}Mo $8^+ \to 6^+$, ^{92}Mo $6^+ \to 4^+$, and ^{93}Tc $\frac{21}{2}^+ \to \frac{17}{2}^+$, rather consistent proton effective charges are obtained with an average value $e_p = 1.63 \pm 0.03$. In Sec. IV D, the neutron effective charge is discussed and a brief comparison with the proton and neutron effective charges needed in other regions of spherical nuclei is presented.

In ^{91}Nb the $E2/M1$ mixing ratios for the 2661-keV $(\frac{15}{2}^-, \frac{19}{2}^-) \to$ 2035-keV $\frac{17}{2}^-$, and 2414-keV $\frac{11}{2}^- \to$ 1985-keV $\frac{13}{2}^-$ transitions have been measured. If these states are assumed to have the $(g_{9/2})^2 p_{1/2}$ configurations as indicated in Fig. 8, the mixing ratios can be related to the ratio of the quadrupole moment of the state $(g_{9/2})^2 J_0$ to the difference of the $g_{9/2}$ and $p_{1/2}$ g factors:

$$\delta(E2/M1) = -\frac{E_\gamma(\mathrm{MeV})}{120}\frac{\langle J_f \| E2 \| J_i\rangle}{\langle J_f \| M1 \| J_i\rangle} = -\frac{E_\gamma(\mathrm{MeV})}{240}\frac{\sqrt{5}}{J_0}\left(\frac{2J_0+3}{2J_0-1}\right)^{1/2}\left(\frac{Q(J_0)}{g(g_{9/2})-g(p_{1/2})}\right).$$

The theoretical mixing ratios were calculated with an effective charge of $e_p = 1.35$ and empirical g factors measured for the $g_{9/2}$ and $p_{1/2}$ configurations in ^{89}Y and ^{90}Zr.[31,41] The results are compared with the experimental mixing ratios in Table V. The agreement with experiment is very good for the theoretical $\frac{15}{2}^- \to \frac{17}{2}^-$ result, but the large mixing ratio observed for the $\frac{11}{2}^- \to \frac{13}{2}^-$ transition cannot be explained with any reasonable value for the $J_0 = 6^+$ quadrupole moment. This disagreement may be due to a misassignment of part of the 430-keV γ ray to the $\frac{11}{2}^- \to \frac{13}{2}^-$ transition in the present and previous experiments[21] or to a different structure for the 2414-keV $\frac{11}{2}^-$ level.

C. ^{91}Zr and $N = 51$ energy levels

The low-lying ^{91}Zr energy levels are characterized by multiplets of levels formed from the coupling of the $N = 51$ single-particle neutron states to the ^{90}Zr energy levels. The levels in ^{91}Zr which have the largest single-particle spectroscopic factors in the ^{90}Zr(d,p) experiments[22-24] are 0-keV $\frac{5}{2}^+$ $(2d_{5/2})$, 1205-keV $\frac{1}{2}^+$ $(3s_{1/2})$, 2041-keV $\frac{3}{2}^+$ $(2d_{3/2})$, 2170-keV $\frac{11}{2}^-$ $(1h_{11/2})$, and 2201-keV $\frac{7}{2}^+$ $(1g_{7/2})$. In addition, the $\frac{9}{2}^+$ level at 2905 keV observed in ^{92}Zr(p,d) experiments[22,42] has been suggested to have the structure $^{92}\mathrm{Zr} \otimes g_{9/2}^{-1}$ or approximately $^{90}\mathrm{Zr} \otimes [(d_{5/2})^2, g_{9/2}^{-1}]$.

A comparison between experimental and theoretical energy levels for ^{90}Zr and ^{91}Zr is shown in Fig. 9. Taking into account the fact that some

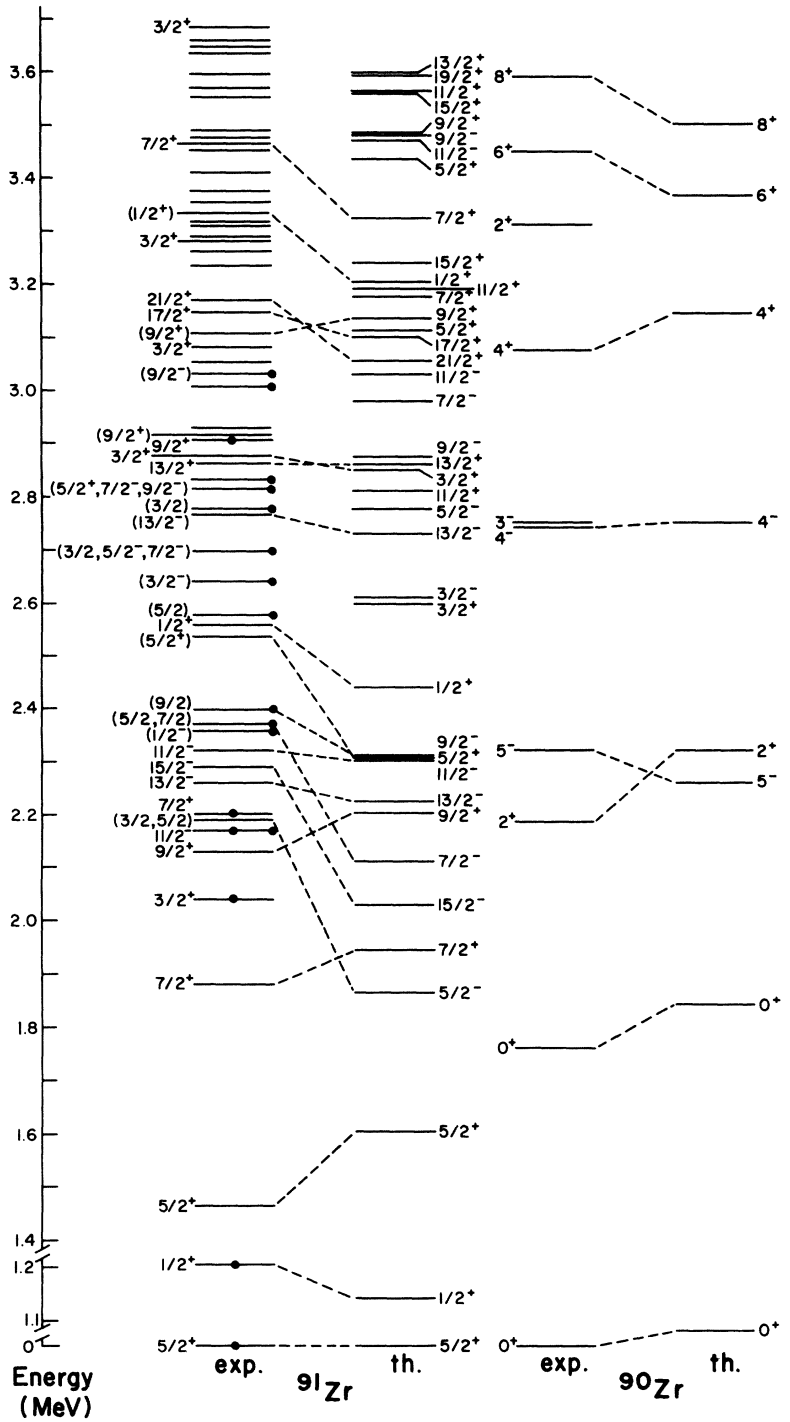

FIG. 9. Comparison of experimental and theoretical energy levels for ^{91}Zr and ^{90}Zr. The experimental levels for ^{91}Zr are from the present experiment and Refs. 17 and 22–25. The experimental levels for ^{90}Zr are from Ref. 31. The ^{91}Zr experimental levels marked with a dot in the middle have been observed with large single-particle and single-hole spectroscopic factors in (d,p) and (p,d) reactions (Refs. 22–24 and 42). The ^{91}Zr experimental levels marked with a dot on the right have been observed with $L=3$ angular distributions in (p,p') experiments (Ref. 22) which indicate that they have some component of the weak coupling multiplet based on the ^{90}Zr 3^- state. The theoretical levels have been calculated by Gloeckner *et al.* for ^{90}Zr (Ref. 11) and ^{91}Zr (Ref. 40) based on the interaction discussed in Sec. IV of the text. Only the $2d_{5/2}$ and $3s_{1/2}$ neutron single-particle levels have been considered in the theoretical calculation. Other single-particle neutron levels as well as the 3^- and second 2^+ levels in ^{90}Zr are outside the theoretical model space.

states are not included within the basis used for the theoretical shell-model calculation, the over-all comparison between theory and experiment is good, the worst deviation being about 300 keV. Shell-model calculations for the $\frac{21}{2}^+$ and $\frac{17}{2}^+$ high-spin states in ^{91}Zr which were carried out about ten years ago [see Auerbach and Talmi[4] (p. 474) and Vervier[3] (p. 53)] as well as the recent theoretical calculation of Gloeckner *et al.*, shown in Fig. 9, predict the $\frac{21}{2}^+$ state to lie below the $\frac{17}{2}^+$ state, creating an $E4$ isomer similar to the one predicted and found experimentally in ^{93}Mo. The $\frac{21}{2}^+$ state has in fact been found in the present experiment to lie above the $\frac{17}{2}^+$ state; however, this disagreement with theory (a difference of about 120 keV for the $\frac{21}{2}^+$ state) is not particularly worse than that for other positive-parity states. An interaction which gives the correct ordering of the ^{91}Zr high-spin has been reported,[15,40] but this interaction apparently gives a worse over-all agreement with the other $N=51$ isotones.

It is interesting to compare the systematics of the positive-parity levels in the even-even $N=50$ isotones and the neighboring even-odd $N=51$ isotones (see Fig. 10). Theoretically, the assumed $(g_{9/2})^n(\nu=2)$ seniority-2 structure of the even-even $N=50$ isotones has spacings between the $J=2^+$, 4^+, 6^+, and 8^+ levels which are independent of n. The worst deviation from the theoretical calculation is observed for ^{90}Zr. Similarly, the worst deviation for the $N=51$ nuclei occurs for the neighboring ^{91}Zr nucleus. On the other hand, the experimental-theoretical agreement is very good for both the ^{94}Ru and ^{95}Ru isotopes and reasonably good for the ^{92}Mo and ^{93}Mo isotopes. Thus, the deviations for ^{90}Zr and ^{91}Zr to a large extent result from the discrepancy in the proton-proton interaction. From the observation that the spacings of the energy levels for the ^{95}Ru positive-parity yrast states are very similar to the spacings in ^{94}Ru, one may expect that the positive-parity yrast levels for other nearby nuclei can be very well predicted from a simple weak-coupling model in which the proton-neutron interaction is ignored.

Three sets of sextuplets are expected in ^{91}Zr from the couplings of the $d_{5/2}$ neutron with the 3^-, 4^-, and 5^- states in ^{90}Zr. *A priori*, the states of the same spin from the different multiplets may be mixed. The theoretical prediction for the lowest five states, which naively is expected to be the 5^- multiplet, is in relatively poor agreement with experiment even for the unique $\frac{15}{2}^-$ high-spin state (see Fig. 9). Other theoretical predictions[3,12] based on slightly different effective interactions do not give better agreement. The (p,p') experiment of Blok[22] gives additional information concerning the wave function components coupled to the ^{90}Zr 5^- state since the components containing the ^{90}Zr 4^- configuration are excited only very weakly, because a spin flip is involved. Blok observed states with $L=5$ at 2.189, 2.261, 2.289, 2.322, 2.369, and 2.766 MeV. The states at 2.261 and 2.766 MeV are both assigned $\frac{13}{2}^-$ in the present experiment. The largest $L=5$ (p,p') component is observed for the upper $\frac{13}{2}^-$ state contrary to naive expectations based on the ordering of the 4^- and 5^- ^{90}Zr states. However, this reverse mixing of the two $\frac{13}{2}^-$ states is supported by the small $B(M1)_{\text{exp}}$

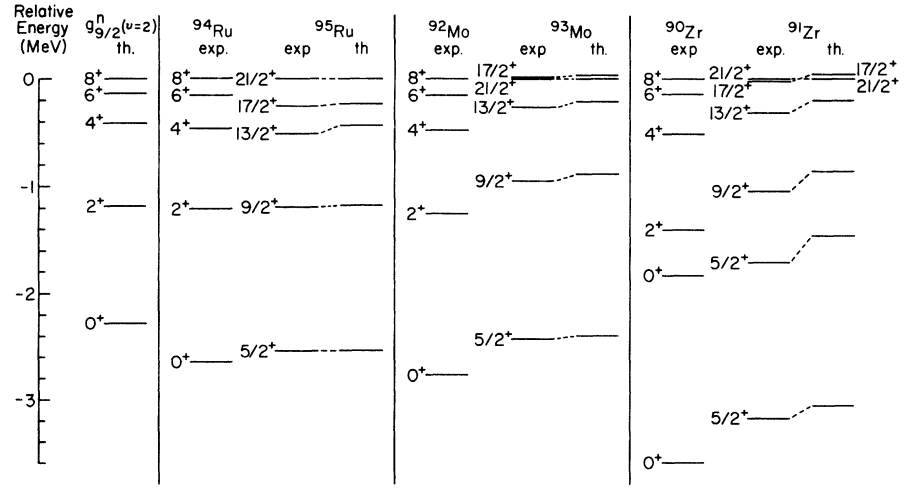

FIG. 10. A comparison of the systematics for the positive-parity yrast levels in the even-even $N=50$ nuclei and in the adjacent $N=51$ nuclei. The theoretical energy levels were obtained by Gloeckner *et al.* (Refs. 11 and 40) using the effective interaction discussed in Sec. IV of the text. The experimental levels for ^{91}Zr are from the present work and the levels for other nuclei are from Refs. 5, 6, 16, 31, and 37.

TABLE VI. $B(E2)$ values for $N=51$ nuclei.

Nucleus	$J_i \to J_f$	$\tau(J_i)$	E_γ (keV)	Branching ratio (%)	ICC [a]	$B(E2)_{\exp}$ [a] (e^2 fm^4)	Proton [b] configuration	$B(E2)_{th} = (Ae_p + Be_n)^2$ [c] A (fm^2)	B (fm^2)	e_p [d] from $N=50$	e_n [e]
^{91}Zr	$\frac{21}{2}^+ \to \frac{17}{2}^+$	6.28 ± 0.20 μsec [f]	20.4	96.2	316	111 ± 6	$g_{9/2}{}^2$	3.55	3.53	1.91 ± 0.05	1.06 ± 0.10
^{92}Nb	$5^+ \to 7^+$	2.73 ± 0.09 nsec [g]	357	100	0.012	50.7 ± 1.7	$g_{9/2}p_{1/2}{}^2 + g_{9/2}{}^3$	1.25	5.57	1.79 ± 0.09	0.88 ± 0.04
	$11^- \to 9^-$	241 ± 5 nsec [h]	115.4	100	0.690	98 ± 3	$g_{9/2}{}^2 p_{1/2}$	3.61	3.03	1.35 ± 0.04	1.66 ± 0.06
^{93}Mo	$\frac{17}{2}^+ \to \frac{13}{2}^+$	5.09 ± 0.26 nsec [i]									
		5.6 ± 0.4 nsec [h]									
	Average	5.3 ± 0.3	268	100	0.033	108 ± 6	$g_{9/2}{}^2 p_{1/2}{}^2 + g_{9/2}{}^4$	5.01	2.25	1.62 ± 0.03	1.01 ± 0.15

[a] See footnotes to Table IV.
[b] The neutron configuration space is $(2d_{5/2}, 3s_{1/2})$.
[c] $B(E2)_{th}$ from Refs. 12 and 40; $\nu = 0.212$ for the radial matrix elements.
[d] Typical values from Table IV.
[e] $e_n = [B(E2)_{exp}{}^{1/2} - Ae_p]/B$.
[f] Present experiment.
[g] S. Cochavi and D. B. Fossan, Phys. Rev. C 3, 275 (1971).
[h] Reference 16.
[i] C. Günther, M. V. Banaschik, H. Hübel, W. D. Schneider, K. H. Gonsoir, and P. Herzog, Nucl. Phys. A244, 287 (1975).

$= [(6.8 \pm 0.4) \times 10^{-3}]\mu_N{}^2$ obtained for the 2287-keV $\frac{15}{2}^- \to$ 2259-keV $\frac{13}{2}^-$ transition. Assuming the wave functions

$$|\tfrac{15}{2}^-\rangle = |(^{90}\mathrm{Zr}\ 5^-)(\nu d_{5/2})\rangle ,$$

$$|\tfrac{13}{2}^-\rangle = \alpha\,|(^{90}\mathrm{Zr}\ 4^-)(\nu d_{5/2})\rangle + (1-\alpha^2)^{1/2}\,|(^{90}\mathrm{Zr}\ 5^-)(\nu d_{5/2})\rangle$$

and using empirical g factors[41] for the $M1$ matrix elements, the calculated $B(M1)$ is $1.20\mu_N{}^2$ for $\alpha^2 = 0$ and $0.29\mu_N{}^2$ for $\alpha^2 = 1$. The small observed $B(M1)_{exp}$ can only be obtained from destructive interference between these limits for $\alpha^2 \approx 0.80$; that is, if the lowest $\frac{13}{2}^-$ level has mostly the 4^- multiplet component.

Twelve levels below 3.2 MeV were observed with $L=3$ in the (p,p') experiment[22] which indicates that they contain components of the ^{90}Zr 3^- level which is strongly excited by inelastic excitation. Since only six states are expected for the 3^- multiplet, considerable mixing between the wave functions for 3^-, 4^-, and 5^- components must occur. The mixing of the $\frac{11}{2}^-$ member of the 3^- multiplet with the $1h_{11/2}$ single-particle level is very similar to the situation in ^{209}Pb with regard to the $1j_{15/2}$ orbital which has been theoretically discussed by Hamamoto.[43] This mixing has also been discussed for the neighboring $N=51$ odd-even nucleus ^{89}Sr [8] where the enhanced $\frac{11}{2}^- \to \frac{5}{2}^+$ $E3$ transition can be explained with about equal admixtures of the $1h_{11/2}$ single-particle and the $(^{88}\mathrm{Sr}\ 3^-) \otimes (\nu d_{5/2})$ components.

D. ^{91}Zr and $N=51$ $B(E2)$ values

The $B(E2)$ value for the highly converted ^{91}Zr $\frac{21}{2}^+ \to \frac{17}{2}^+$ 20.4-keV transition can be calculated from the present lifetime measurement for the $\frac{21}{2}^+$ state together with the theoretical internal conversion coefficient (ICC) interpolated from the tables of Hager and Seltzer.[30] Even though $E_\gamma{}^5$ and the ICC are individually very sensitive to the transition energy, the product $E_\gamma{}^5(1+\mathrm{ICC})$ which is used in deducing the experimental $B(E2)$ value is relatively insensitive. The deduced $B(E2)$ value is

$$B(E2)[^{91}\mathrm{Zr}\ \tfrac{21}{2}^+ \to \tfrac{17}{2}^+] = 111 \pm 6\ e^2\,\mathrm{fm}^4 ,$$

where most of the error comes from an estimated 5% uncertainty in the theoretical ICC.

This ^{91}Zr $B(E2)$ value and the few other $B(E2)$ values which are known for $N=51$ nuclei are compared with the theoretical calculations of Gloeckner[12] in Table VI. The theoretical $B(E2)$ values are given in the form $(Ae_p + Be_n)^2$. The neutron effective charge is deduced for each transition assuming a proton effective charge given by the average value needed for the equivalent proton configu-

ration in the neighboring $N=50$ nucleus (see Table IV).

Similar to the situation for the $N=50$ proton effective charges discussed in Sec. IV B, considerable variation is found for the $N=51$ neutron effective charges. In this case the variation may be due to the $2d_{3/2}$ and $1g_{7/2}$ neutron-particle orbitals which have not been included in the model space. *A priori*, the influence of these orbitals cannot be excluded from any of the transitions included in Table VI. A typical $N=51$ neutron effective charge, which will be used below for comparison with values for other mass regions, will be taken from the transition involving the simplest configuration considered, namely the ^{91}Zr $\frac{21}{2}^+ \rightarrow \frac{17}{2}^+$ transition for which $e_n = 1.06 \pm 0.10$ was deduced. This value is consistent with the neutron effective charges needed for the Zr isotopes using a $(2d_{5/2}, 3s_{1/2})$ neutron shell-model description.[12]

Finally, it is interesting to compare the average proton and neutron $E2$ effective charges deduced for the mass-90 region, $e_p = 1.63 \pm 0.03$ (see Sec. IV B) and $e_n = 1.06 \pm 0.10$ with effective charges for transitions between high-spin states in other spherical regions. These mass-90 values are quite similar, but a little larger than the effective charges in the ^{208}Pb region,[39] $e_p = 1.53 \pm 0.04$ and $e_n = 0.73 \pm 0.04$ for the $2g_{9/2}$ orbital; whereas they are smaller than the effective charges in the ^{56}Ni region, $e_p = 1.98 \pm 0.10$[38] and $e_n = 1.70 \pm 0.08$.[44] To the extent that the effective charges can be described by a coupling of the valence particles to $\Delta N=2$ $J=2^+$ core excitations (N refers to a major harmonic oscillator shell), which make up the giant quadrupole states, the values are expected to exhibit a simple mass dependence. This mass dependence of the effective charges is estimated in the macroscopic model[45] as $e_{t_z} = (\frac{1}{2} - t_z) + Z/A + 0.64 t_z Z/A$, where $t_z = -\frac{1}{2}$ for a proton and $\frac{1}{2}$ for a neutron. This estimate is in best agreement with the deduced effective charges for the ^{208}Pb region, but in all cases predicts proton and neutron effective charges that are smaller than the deduced values. However, in the cases considered above for the ^{56}Ni, mass-90, and ^{208}Pb regions, the analyses have been carried out within model spaces which have been truncated even within one major oscillator shell, which introduces additional variations in the effective charge. The model space dependence of the effective charge for the nuclei near the ^{16}O and ^{40}Ca closed cores, which are in addition complicated by large core-deformed ($\Delta N=1$) components, has been discussed in detail previously.[38] Recently, microscopic calculations for the ^{208}Pb region which include both the $\Delta N=0$ and $\Delta N=2$ contributions have been carried out which give good agreement for the effective charges.[46] It would be interesting to carry out similar microscopic calculations for the mass-90 region and to study separately the $\Delta N=0$ and $\Delta N=2$ contributions in order to establish a correspondence with the macroscopic models.

The authors would like to acknowledge the help of R. McKeown with the data analysis.

---

*Work supported in part by the National Science Foundation.

†Present address: Michigan State University, East Lansing, Michigan.

‡Present address: Brooklyn College of The City University of New York, Brooklyn, New York.

[1]S. Bjørnholm, O. B. Nielsen, and R. K. Sheline, Phys. Rev. 115, 1613 (1959).

[2]K. W. Ford, Phys. Rev. 98, 1516 (1955); B. F. Bayman, A. S. Reiner, and R. K. Sheline, *ibid.* 115, 1627 (1959).

[3]J. Vervier, Nucl. Phys. 75, 17 (1966).

[4]N. Auerbach and I. Talmi, Nucl. Phys. 64, 458 (1965).

[5]D. N. Kundu, J. L. Hult, and M. L. Pool, Phys. Rev. 77, 71 (1950); D. C. Kocher, Nucl. Data B8, 527 (1972).

[6]C. M. Lederer, J. M. Jaklevic, and J. M. Hollander, Nucl. Phys. A169, 449 (1971); A169, 489 (1971); J. M. Jaklevic, C. M. Lederer, and J. M. Hollander, Phys. Lett. 29B, 179 (1969).

[7]M. Grecescu, A. Nilsson, and L. Harms-Ringdahl, Nucl. Phys. A212, 429 (1973).

[8]A. Nilsson and M. Grecescu, Nucl. Phys. A212, 448 (1973); S. E. Arnell, A. Nilsson, and O. Stankiewicz, *ibid.* A241, 109 (1975).

[9]J. B. Ball, J. B. McGrory, and J. S. Larsen, Phys. Lett. 41B, 581 (1972); F. J. D. Serduke, R. D. Lawson, and D. H. Gloeckner, Nucl. Phys. (to be published); D. H. Gloeckner, Phys. Lett. 42B, 381 (1972).

[10]D. H. Gloeckner, M. H. Macfarlane, R. D. Lawson, and F. J. D. Serduke, Phys. Lett. 40B, 597 (1972).

[11]D. H. Gloeckner and F. J. D. Serduke, Nucl. Phys. A220, 477 (1974).

[12]D. H. Gloeckner, Nucl. Phys. A253, 301 (1975).

[13]J. O. Newton, in *Nuclear Spectroscopy and Reactions, Part C*, edited by J. Cerny (Academic, New York, 1974), pp. 185–227; J. R. Grover, Phys. Rev. 157, 832 (1967).

[14]B. A. Brown, P. M. S. Lesser, and D. B. Fossan, Bull. Am. Phys. Soc. 18, 1416 (1973); in *Proceedings of the International Conference on Nuclear Structure and Spectroscopy, Amsterdam, 1974*, edited by H. P. Blok and A. E. L. Dieperink (Scholar's Press, Amsterdam, 1974), Vol. 1, p. 90.

[15]B. A. Brown, P. M. S. Lesser, and D. B. Fossan, Phys. Rev. Lett. 34, 161 (1975).

[16]B. A. Brown, D. B. Fossan, P. M. S. Lesser, and A. R. Poletti, in *Proceedings of the International Conference on Nuclear Structure and Spectroscopy, Amsterdam, 1974* (see Ref. 14), p. 94; Phys. Rev. C 13,

1194 (1976); Progress Report, SUNY at Stony Brook, 1975; and (unpublished).
[17]H. Verheul and W. B. Ewbank, Nucl. Data. B8, 477 (1972).
[18]S. Matsuki, S. Nakamura, H. Hyakutake, M. Matoba, Y. Yosida, and I. Kumabe, Nucl. Phys. A201, 608 (1973).
[19]F. Rauch, Z. Phys. 243, 105 (1971).
[20]C. V. K. Baba, D. B. Fossan, T. Faestermann, F. Feilitzsch, M. R. Maier, P. Raghavan, R. S. Raghavan, and C. Signorini, J. Phys. Soc. Jpn. Suppl. 34, 260 (1973); Nucl. Phys. A257, 135 (1976).
[21]A. Berinde, R. O. Dumitru, M. Grecescu, A. Iordachescu, I. Neamu, G. Pascovici, D. Ploştinaru, and C. M. Teodorescu, Z. Phys. 269, 117 (1974).
[22]H. P. Blok, Thesis, Vrije Universiteit, Amsterdam, 1972 (unpublished); H. P. Blok, L. Hulstman, E. J. Kaptein, and J. Blok (unpublished).
[23]M. R. Maier, thesis, Technische Universität, München, 1972 (unpublished).
[24]A. Graue, L. H. Herland, K. J. Lervik, J. T. Nesse, and E. R. Cosman, Nucl. Phys. A187, 141 (1972).
[25]J. E. Glenn, H. W. Baer, and J. J. Kraushaar, Nucl. Phys. A165, 533 (1971).
[26]T. Yamazaki, Nucl. Data A3, 1 (1967).
[27]J. O. Rasmussen and T. T. Sugihara, Phys. Rev. 151, 992 (1966); Z. P. Sawa, Phys. Scr. 7, 5 (1973).
[28]H. W. Baer, R. L. Bunting, J. E. Glenn, and J. J. Kraushaar, Nucl. Phys. A218, 355 (1974).
[29]R. E. Holland, R. D. Lawson, and F. J. Lynch, Ann. Phys. (N.Y.) 63, 607 (1971).
[30]R. S. Hager and E. C. Seltzer, Nucl. Data A4, 1 (1968).
[31]D. C. Kocher, Nucl. Data Sheets 16, 55 (1975).
[32]K. G. Lobner, Nucl. Phys. 58, 49 (1964).
[33]For recent review articles concerning the theoretical foundations for effective operators see D. S. Koltun, Annu. Rev. Nucl. Sci. 23, 163 (1973); S. Yoshida and L. Zamick, *ibid.* 22, 121 (1972); B. R. Barrett and M. W. Kirson, in *Advances in Nuclear Physics*, edited by M. Baranger and E. Vogt (Plenum, New York, 1973), Vol. 6, p. 219.
[34]See the following reference for a further discussion of the correlation between the level structure of the $p_{1/2}$ doublets and the properties of the residual interaction: Iu. I. Kharitonov, L. K. Peker, and L. A. Sliv, Phys. Lett. 31B, 277 (1970).
[35]W. D. Schneider, K. H. Gonsior, and C. Günther, Nucl. Phys. A249, 103 (1975).
[36]C. W. DeJager, H. DeVries, and C. DeVries, At. Data Nucl. Data Tables 14, 479 (1974).
[37]S. Cochavi, J. M. McDonald, and D. B. Fossan, Phys. Rev. C 3, 1352 (1971).
[38]B. A. Brown, D. B. Fossan, J. M. McDonald, and K. A. Snover, Phys. Rev. C 9, 1033 (1974).
[39]G. Astner, I. Bergström, J. Blomqvist, B. Fant, and K. Wikström, Nucl. Phys. A182, 219 (1972).
[40]D. H. Gloeckner (private communication).
[41]V. S. Shirley, in *Hyperfine Interactions in Excited Nuclei*, edited by G. Goldring and R. Kalish (Gordon and Breach, New York, 1971), Vol. 4, p. 1266.
[42]J. B. Ball and C. B. Fulmer, Phys. Rev. 172, 1199 (1968).
[43]I. Hamamoto, Nucl. Phys. A126, 545 (1969).
[44]P. W. M. Glaudemans, M. J. A. Voigt, and E. F. M. Steffens, Nucl. Phys. A198, 609 (1972).
[45]I. Hamamoto, Phys. Scr. 6, 266 (1972).
[46]P. Ring, R. Bauer, and J. Speth, Nucl. Phys. A206, 97 (1973).